December 2012

An Investigation of the Through-Thickness Stress Intensity Factor Using P- and H-Element Finite Element Analysis

Christopher Castle
University of Wisconsin-Milwaukee

AN INVESTIGATION OF THE THROUGH-THICKNESS STRESS INTENSITY FACTOR USING P- AND H-ELEMENT FINITE ELEMENT ANALYSIS

by

Christopher Castle

A Thesis Submitted in

Partial Fulfillment of the

Requirements for the Degree of

Master of Science

in Engineering

at

The University of Wisconsin-Milwaukee

December 2012

ABSTRACT

AN INVESTIGATION OF THE THROUGH-THICKNESS STRESS INTENSITY FACTOR USING P- AND H-ELEMENT FINITE ELEMENT ANALYSIS

by

Christopher Castle

The University of Wisconsin-Milwaukee, 2012

The stress intensity factor is used in fracture mechanics to characterize the stress state near the crack tip in a structure under remotely applied loads. The magnitude of the stress intensity factor is dependent on geometry, the size and location of the crack, and the magnitude and distribution of loads on the structure. The scope of this thesis is the study of the through-thickness stress intensity factor using two different FE approaches. *P*- and *h*-element finite element methods are used to study the stress intensity factors. The accuracy of the predicted Mode I stress-intensify factor (K_I) is assessed using closed-form and planar analysis approaches. The research also contains studies on how plate thickness, element formulations, and materials affect K_I, as well as possible relationships between the through-thickness K_I and K_C, the critical stress intensity factor.

TABLE OF CONTENTS

LIST OF FIGURES

LIST OF TABLES

LIST OF ABBREVIATIONS

E: Young's modulus

G: Energy release rate

J: J Contour Integral

K: Stress intensity factor

K_C: Critical stress intensity factor, or fracture toughness

K_I: Mode I stress intensity factor

K_{II}: Mode II stress intensity factor

K_{III}: Mode III stress intensity factor

Γ: Domain integrals

LEFM: Linear elastic fracture mechanics

r: Radial distance from crack tip

SIF: Stress intensity factor

σ_{xx}: Stress in the x-direction

σ_{yy}: Stress in the y-direction

μ: Shear modulus

t: Plate thickness

u = x-direction displacement

v: Poisson's ratio

w: Strain energy density, or z-direction displacement

δ_{ij}: Kronecker delta

1. Introduction

1.1 Introduction

This study investigates the effect of thickness on the determination of the Mode I stress intensity factor. Stress intensity factors, which have units of stress · (length)$^{1/2}$, characterize the stress state ahead of a sharp crack using a single constant value [1]. Stress intensity factors are most often approximated using two-dimensional analysis, but three-dimensional analysis is required to determine if the two-dimensional idealization is acceptable [2]. Stress intensity factors were first developed by Irwin [3], who used Westergard's [4] previous research as a basis for his work. Stress intensity factors are important as they provide a means for determining when fracture will take place, which occurs when the stress intensity factor equals the material's fracture toughness [1]. The investigation is performed using *p*-element and *h*-element finite element analyses. These two methods were chosen as they are the two most common finite element techniques. Three-dimensional results from both methods are compared to one another and to two-dimensional analyses. This section presents the theoretical background on the three-dimensional stress intensity factor determination.

1.2 Research objectives and methodology

The primary objective of this research is to compare the through-thickness Mode I stress intensity factors (K_I) calculated using two fundamentally different finite element (FE) approaches. The *h*-element method is based on a fixed polynomial order whereas the *p*-element is based on increasing the polynomial order. The aim is to understand the

variation in results based on using these two approaches. The goal of the investigation is to:

- Understand how the stress intensity factor, K_I varies through the thickness of plates which may be commonly encountered in engineering practice
- Assess the error associated with using two-dimensional analysis and closed form solutions to determine the stress intensity factor in a cracked, three-dimensional structure

The following sections describe some of the key research carried out in the area and the research methodology. Three-dimensional finite element models will be analyzed using two different methods, specifically the *h*-element and *p*-element methods. These models will be used to make comparisons between the two approaches for a number of common plate thicknesses. Two-dimensional finite element models will also be constructed to compare the error that may be associated with making planar assumptions. Research in the effects of related topics such as element technology and the use of various common engineering materials will also be included.

2. Literature review

The following literature review covers the basic principles of linear elastic fracture mechanics important to this research and a summary of the theoretical framework underlying the *h*- and *p*-element methods. It also reviews previous research on the topic of three-dimensional stress intensity factors.

2.1 Plane stress versus plane strain

A common practice in stress analysis is to assume a specimen is in a two-dimensional, planar state of stress. This two-dimensional state can be described as either plane stress or plane strain. Plane stress is defined as a state of stress in which the normal stress, σ_Z, and the shear stresses σ_{XZ} and σ_{YZ} directed perpendicular to the x-y plane are assumed to be zero [1]. More simply put, two faces of a cubic element are stress free [5] (see Figure 1).

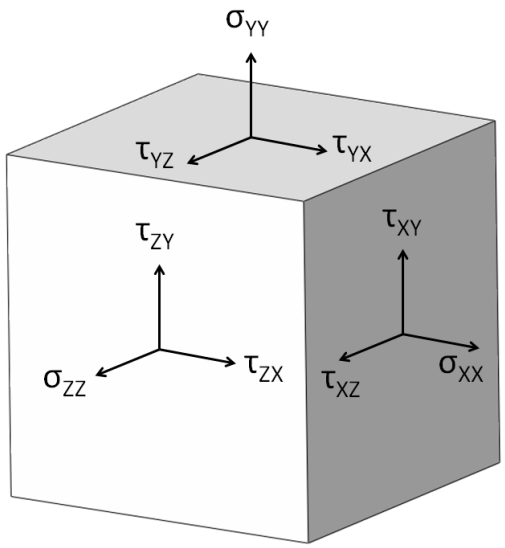

Figure 1: Stress tensor at a point in space

Plane stress occurs most often for very thin isotropic plates subjected to only in-plane loads [1]. Considering a cracked plate, the region near the crack typically experiences plane stress conditions if the crack length is large compared to the plate thickness [6]. Conversely, plane strain is described by the condition in which the strain normal to the x-y plane, ε_Z, and the shear strains γ_{XZ} and γ_{YZ} are assumed to be zero. Plane strain often occurs when a specimen is much thicker in one direction (for example the z direction) than in the other two (x and y) directions [1]. For a cracked plate plane

strain conditions typically prevail near the crack when the crack length is small compared to the plate thickness [6].

However, real structures seldom behave in purely plane strain or plane stress ways. This is especially true in cracked structures, where local constraints near the crack tip cause increases in stress intensity. This increase in stress intensity is often ignored in analysis, which usually assumes constant stress through the thickness [7]. Stresses are not uniform through the thickness, and can only be accurately analyzed using three-dimensional analysis [8].

Bakker showed that a cracked plate under plane stress undergoes a change to plane strain behavior near the crack tip [7]. He states that this change occurs at $r/t < 0.5$, and is confirmed by Nakamura for a sufficiently thin plate [9]. Nakamura goes further to say that this transitional region extends to a radial distance from the crack front of about one and one-half times the plate thickness. Bakker [7] adds that the radial position where the plane stress to plane strain transition takes place strongly depends on the position in the thickness direction.

2.2 Elementary fracture mechanics & stress intensity factor

Fracture mechanics is that technology concerned with the modeling of cracking phenomena [10]. Paris [11] stated that "the high elevation of stresses near the tip of a crack should receive the utmost attention, since it is at that point that additional growth of the crack takes place." The topics that follow give the basis for making such evaluations.

For a plate with a through-thickness crack, the loading on the crack is typically described as one of three types, or modes (Figure 2). Mode I describes an opening of the crack, with the applied tensile load normal to the crack plane (cleavage), and will be the

focus of this research. Mode II describes in-plane shear, and Mode III describes out-of-plane shear (tearing). In addition, the crack may be simultaneously subjected to a combination of these loading modes, known as mixed mode loading.

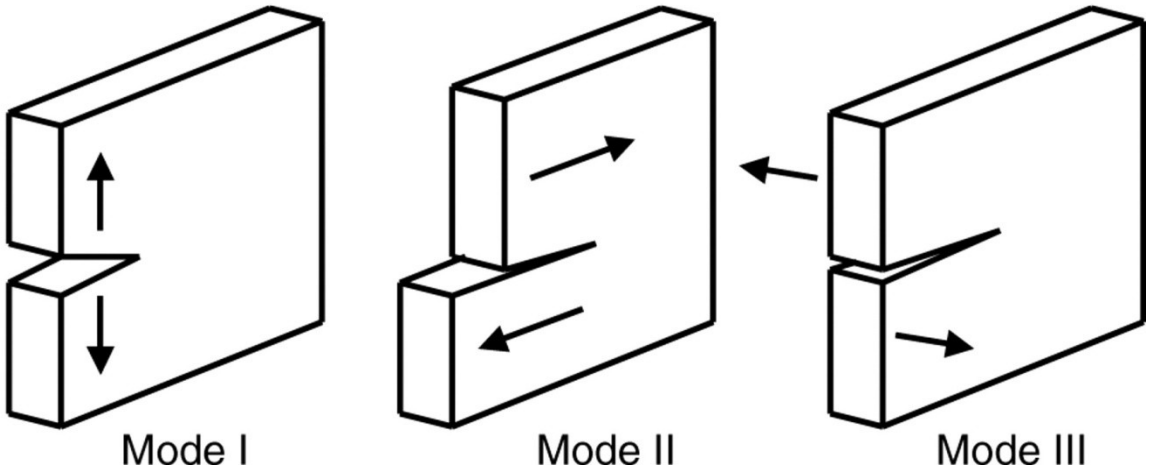

Figure 2: Crack opening modes

The geometries of cracks, with radius of curvatures approaching zero at the crack tip, cause stress fields that approach infinity proportional to the reciprocal of the square root of the distance from the crack tip [12]. This occurs even at low load levels. As such, commonly used failure measures such as von Mises are not applicable [13]. The stress intensity factor (*K*, or *SIF*) was first proposed by Irwin in 1957 [14] and can be thought of as a measure of the effective local stress at the crack tip [15]. An increasing *K* indicates the stress near the crack tip is increasing. With this linear elastic fracture mechanics approach of characterizing the crack tip stresses, small amounts of plasticity may be viewed as taking place within the crack tip stress field and neglected for the characterization [11]. *K* is designated by the mode of loading, such as K_I, K_{II}, and K_{III}.

K is usually expressed in the following units:

$MPa\sqrt{m}$ for metric units

$ksi\sqrt{in}$ for imperial units

K can be determined using closed-form solutions, finite element analysis, and a number of other techniques. The solutions relate the remote loading, geometry of the specimen, and the crack size to the stress intensity factor, *K*. Using the stress intensity factor in design requires knowledge of the critical stress intensity factor or fracture toughness (K_C).

The critical stress intensity factor or fracture toughness (K_C) is a mechanical property that measures a material's resistance to fracture. Fracture toughness is used in structural integrity assessment, damage tolerance design, fitness-for-service evaluation, and residual strength analysis [14]. K_C is further expressed according to the loading mode, such as K_{IC}, K_{IIC}, K_{IIIC} for modes one, two, and three, respectively. When the stress intensity factor reaches the material's fracture toughness an existing crack will undergo unstable crack extension [16]. Since K_C is material specific its value must be determined for each material of concern. Further, K_C can vary with temperature, component thickness, and strain rate. Table 1 lists critical stress intensity factors for some common materials [17].

Table 1: Critical stress intensity factors for common materials

	K_C	
	MPa √m	ksi √in
Steel AISI 4340	59	53.7
Stainless Steel AISI 403	77	70.1
Aluminum 2024-T851	23	20.9
Titanium Ti-6AI-6V	66	60.1

The critical stress intensity factor, K_C, is strongly dependent on plate thickness [10]. For thin plates it is often the case that the plastic zone around a crack is on the order of the plate thickness. This allows K_C to reach a maximum value ($K_{C(max)}$). As plate thicknesses increase the size of the plastic zone decreases, lowering the toughness of the material to some level below $K_{C(max)}$. As plate thicknesses continue to increase the plastic zone size becomes constant and K_C reaches an asymptotic value ($K_{C(min)}$), known as the "plane strain fracture toughness" [14]. This is shown in Figure 3.

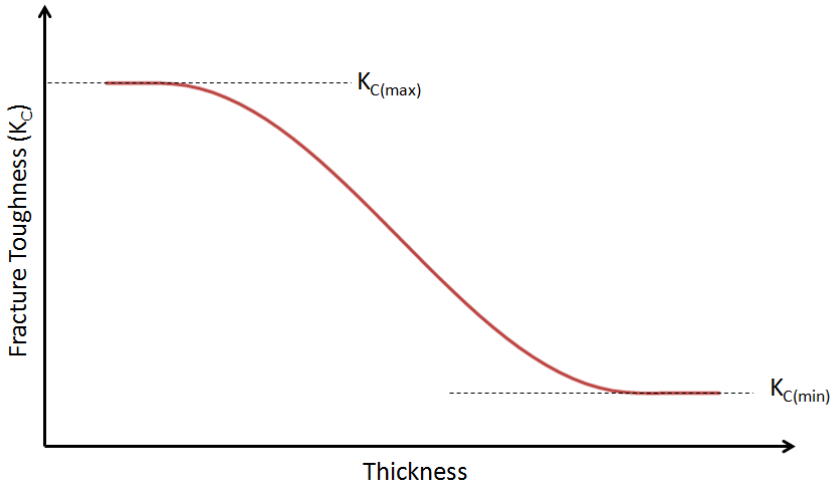

Figure 3: Effect of thickness on K_C

The strain energy release rate, *G*, describes the energy required to grow a crack by a unit length in a given material. This quantity can also be determined from numerical and analytical approaches and can be an indirect approach to measure the stress intensity factor. *G* can be calculated from *K* by the following relationship [1]:

$$G = \frac{K_I^2}{E} \qquad \textbf{Equation 1}$$

The stress intensity factor is useful beyond just being able to predict when fracture will occur under monotonic loading. Paris' Law relates the range of stress intensity factors to sub-critical crack growth due to fatigue loading, and is shown below [1]:

$$\frac{da}{dN} = C\Delta K^m \qquad \textbf{Equation 2}$$

where $\frac{da}{dN}$ is the change in crack length per loading cycle

$C \; and \; m$ are material constants

ΔK is the range of stress intensity factors

Linear elastic fracture mechanics is applicable for conditions that develop a relatively small plastic zone. This includes metallic materials at low load levels. It can be also used for certain materials up to the point of fracture, such as high strength steels, precipitation-hardened aluminum, monolithic ceramics, and ceramic composites [1]. Linear elastic fracture mechanics methods are typically applied to nuclear pressure vessels and piping, oil and gas pipelines, petrochemical vessels and tanks, and automotive, ship, and aircraft structures [14].

The J Contour Integral is a generalized version of the energy release rate, *G*, and as such is actually equal to *G*. *J* was first introduced by Rice in 1968 [14] as a path-independent contour integral for the analysis of cracks. *J* extends fracture mechanics beyond limitations set forth for linear elastic fracture mechanics, and can be viewed as both an energy parameter and a stress intensity parameter [1]. *J* can also be defined by its mode, including J_I, J_{II}, and J_{III}.

2.3 Equations for stress intensity factors

Stress intensity factors can be determined for certain cases if the geometry and remote loading is known. The Mode I stress intensity factor can be developed using a stress function approach, assuming plane strain. The derived equations for the crack tip stress field and displacement field are as follows [11]:

$$\sigma_X = \frac{K_I}{\sqrt{2\pi r}}\cos\frac{\theta}{2}\left(1 - \sin\frac{\theta}{2}\sin\frac{3\theta}{2}\right)$$

$$\sigma_Y = \frac{K_I}{\sqrt{2\pi r}}\cos\frac{\theta}{2}\left(1 + \sin\frac{\theta}{2}\sin\frac{3\theta}{2}\right)$$

$$\tau_{XY} = \frac{K_I}{\sqrt{2\pi r}}\sin\frac{\theta}{2}\cos\frac{\theta}{2}\cos\frac{3\theta}{2}$$

$$\sigma_Z = \nu(\sigma_X + \sigma_Y)$$

Equation 3

$$\tau_{XZ} = \tau_{YZ} = 0$$

$$u = \frac{K_I}{G}\sqrt{\frac{r}{2\pi}}\cos\frac{\theta}{2}\left(1 - 2\nu + sin^2\frac{\theta}{2}\right)$$

$$v = \frac{K_I}{G}\sqrt{\frac{r}{2\pi}}\sin\frac{\theta}{2}\left(2 - 2\nu - cos^2\frac{\theta}{2}\right)$$

$$w = 0$$

Higher order terms are neglected in the development of the above equation, and hence it is limited to cases where the crack radius *r* is small compared to dimensions such as the crack length. Only a partial derivation was shown. The full derivation may be found in [11].

For a semi-infinite plate with a through-thickness centered crack and a remote tensile load (Figure 4) the Mode I stress intensity factor is simplified to [1]:

$$K_I = \sigma\sqrt{\pi a} \qquad \textbf{Equation 4}$$

where σ is the applied remote stress and a is the crack length

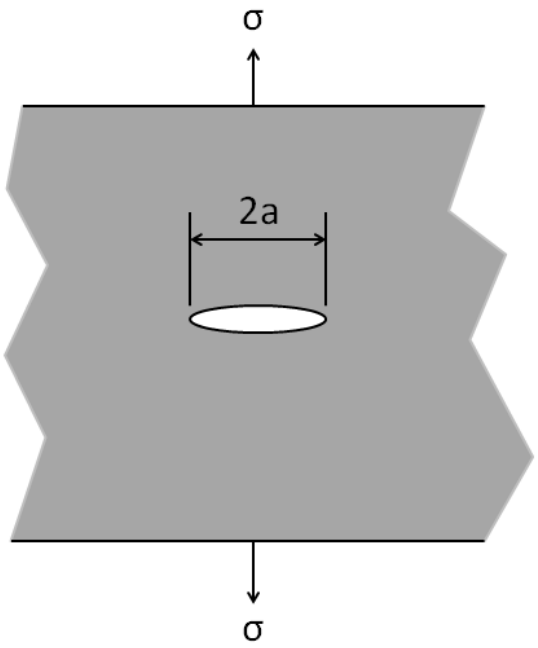

Figure 4: Semi-infinite center-cracked plate

K_I can also be calculated by first solving the *J* integral. The basic equation for doing so is:

$$K_I = \sqrt{J_I E} \qquad \textbf{Equation 5}$$

This equation holds true for plane stress. For plane strain conditions E is replaced by E', where

$$E' = \frac{E}{1 - \nu^2} \qquad \textbf{Equation 6}$$

Equations like those above often assume the crack is small relative to the specimen size, such that the crack-tip is not affected by the external boundaries [7]. For the center-cracked plate studied here, the specimen may be described by the ratio of the crack length to the plate width, a/W. The convention is to describe the full length of the crack as $2a$, and the plate width as $2W$, as shown in Figure 5.

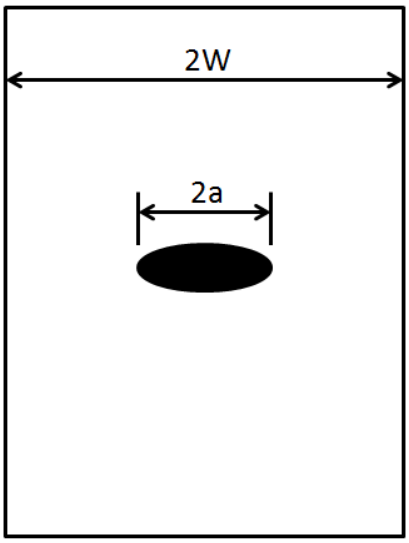

Figure 5: Finite width center-cracked plate

The Mode I stress intensity factor equation for an infinite plate can be modified to include the effect of finite width as shown in the following equation [1]:

$$K_I = \sigma\sqrt{\pi a}\left[\sec\left(\frac{\pi a}{2W}\right)^{\frac{1}{2}}\right]\left[1 - 0.025\left(\frac{a}{W}\right)^2 + 0.06\left(\frac{a}{W}\right)^4\right] \quad \textbf{Equation 7}$$

These stress intensity factor equation solutions typically exist only for fairly simple geometries and loadings. For more complicated scenarios alternate methods must be used, such as finite element analysis.

However, the equations presented above do not satisfy all the three-dimensional equations of elasticity. The assumption that σ_{xx}, σ_{yy}, and σ_{xy} are a function of the x and y coordinates only (assuming z is the through-thickness coordinate), and that the stresses on all z planes are zero violates some of the compatibility equations [6]. For many engineering geometries and loadings the stresses cannot be assumed to remain constant in the component's thickness direction. As such a more rigorous, three-dimensional approach is needed for many real-world situations.

2.4 Crack tip triaxiality & plate thickness

Anderson [1] describes crack tip triaxiality as follows. A thin uncracked plate subjected to in-plane loading would be in a state of plane stress. This is not true for a cracked plate, except for regions sufficiently far from the crack. A single planar assumption, plane stress or plane strain, is not applicable to the entire plate [2]. When a cracked plate is loaded such that an opening load is placed on the crack, a large stress is developed normal to the crack plane. This in turn causes contractions near the crack-tip both in the through-thickness direction and the direction parallel to the crack plane. The material surrounding the crack creates a constraint on such contractions, causing a triaxial

state of stress near the crack-tip. The magnitude of the constraint is dependent on the thickness, size, and configuration of the cracked specimen [14]. In fact this stress triaxiality is not limited to cracks, but is present at other stress raisers as well, such as the case with a hole in an infinite plate [18]. This triaxiality results in stress intensity factors for through-thickness cracked plates that are $(1-\nu^2)^{-0.5}$ times greater than generally reported in stress intensity handbooks [7]. Bakker [7] gives three reasons why a plate that is otherwise in plane stress will experience crack-tip triaxiality:

1. The constraint discussed above causes a plane strain state near the crack tip. Since areas far from the crack tip are in a plane stress state, there must be a transition from plane strain to plane stress state in the vicinity of the crack tip.
2. According to linear elastic fracture mechanics, the singularity at a crack tip is $r^{-0.5}$ at the plate surface of an elastic component. Benthem [19] derived the stresses on a crack front normal to the surface to be singular with $\approx r^{-0.452}$. This implies that the stress intensity factor at the free surface is equal to zero since it is defined as the strength of the $r^{-0.5}$ singularity at the crack tip. The stress intensity factor equaling zero at the free surface is also supported by Yamamoto's research [8].
3. Shear lips formed at the free surface may cause a Mode I crack to become a mixed mode crack.

As such, using a two-dimensional solution to calculate stress intensity factors results in error by a factor of:

$$Error = (1-\nu^2)^{-0.5} \qquad \textbf{Equation 8}$$

For steel with a Poisson's ratio of 0.3, this translates to an error of approximately 4.8 percent. Table 2 lists the Poisson's ratios [20] and errors for common engineering materials.

Table 2: Error in two-dimensional K_I calculation for common materials

material	Poisson's ratio	error, %
cork	0	0.00
concrete	0.2	2.06
cast iron*	0.235	2.88
glass*	0.24	3.01
foam*	0.25	3.28
steel*	0.285	4.33
stainless steel*	0.305	5.00
sand*	0.325	5.74
aluminum alloy	0.33	5.93
copper	0.33	5.93
titanium	0.34	6.33
magnesium	0.35	6.75
clay*	0.375	7.87
gold	0.42	10.19
saturated clay*	0.45	11.98
rubber	0.5	15.47

*average Poisson's ratio

Note that the error in using two-dimensional analysis on cork is zero, meaning that the two-dimensional solution is equal to a three-dimensional solution. This is supported by Yamamoto's research, where he states that a Poisson's ratio of zero causes two-dimensional and three-dimensional solutions to agree [8].

Crack tip triaxiality is also the cause of crack tip tunneling. This phenomenon describes how through-thickness fatigue cracks in plate geometries almost always show crack front tunneling. This scenario can be described by a curved crack front with the deepest point of the crack at the center of the plate [7]. Bakker claims this is because the stress intensity factor is highest at the center of a plate for a straight crack front.

However, the situation where the stress intensity factor is highest at the center of the plate only occurs for relatively thin plates. For thicker plates the stress intensity reaches a peak value just below the free surface [8].

Bakker [7], Benthem [19], and Yamamoto [8] postulate that the stress intensity factor at the free surfaces is equal to zero. However, this claim is still an active area of research. Shivakumar [21], Hartranft and Sih [22], and Sih [6] have studied the intersection between the through-thickness crack and the free surface for over two decades. Shivakumar [21] explains the through-thickness stress field in terms of singularities, stating that there are two dominant singularities impacting the through-thickness response. He states that the first singularity is dominant over the middle 96% if the specimen for a Poisson's ratio of 0.3. The second singularity is dominant at the free surface and quickly diminishes away from the free surface. The thickness of this second singularity boundary layer is approximately 2% of the specimen thickness for a Poisson's ratio of 0.3.

2.5 Finite element analysis techniques

Finite element analysis (FEA) is one of the most powerful and pervasive numerical methods used in modern engineering practice. A central principal of FEA is subdividing the solution domain into smaller, geometrically simple pieces which are called elements, in a process called discretization [15]. An example discretization, or mesh, of a plate with a hole in it is shown in Figure 6.

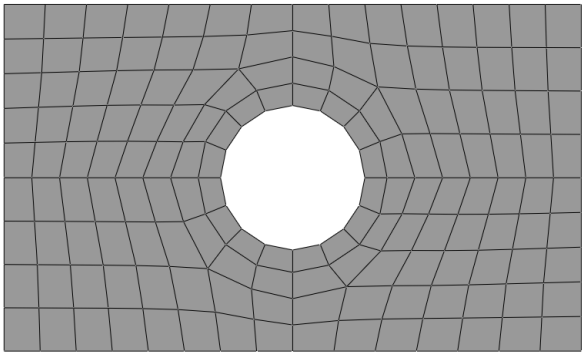

Figure 6: Example of discretization

The finite element method is an approximation of an exact answer and therefore has some amount of error. These errors can come from errors in idealization or discretization, as depicted in Figure 7.

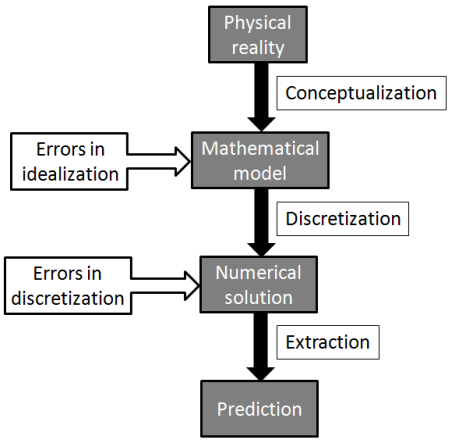

Figure 7: Numerical simulation process [15]

The most common basis of the finite element method used in modern commercial finite element analysis software is known as the *h*-element method, where "*h*" refers to the characteristic length of an element. For an *h*-element analysis, the polynomial degree of any particular element is kept constant throughout the analysis [15]. With the *h*-element approach the discretization error is reduced by increasing the number of elements, thus reducing the characteristic length of the elements. The increase in element

density may be global, or localized to singularities within the model. In order to assure mesh convergence with the *h*-element method the analyst is required to run an initial analysis, then look for regions of high stress (or strain) gradients, and then refine the mesh density in these high gradient areas. If mesh refinement does not change the magnitude of stress or strain significantly after refinement, then the solution in that area is considered converged. If instead the magnitude changes, then additional refinement is done until the stress or strain reaches its asymptotic value. Examples of commercial finite element analysis packages that rely primarily on the *h*-element method include ANSYS [23], Abaqus [24], and Nastran [25].

Another method is known as the *p*-method. In the *p*-element approach the initial mesh is used throughout the analysis. To reduce the discretization error the polynomial degree of the elements is increased [15]. This increase in polynomial degree may be done local to singularities, or consistently throughout the mesh. Incrementally increasing the polynomial degree of the elements is done until stress convergence is realized. This process relieves the user of the need to diligently assure mesh convergence has been achieved. When singularities are present, such as the case with analytical fracture mechanics, *p*-element methods converge with exponential rates if the mesh is properly refined towards the singularities [26]. Two of the most common *p*-element based commercial finite element analysis packages are PTC Creo Simulate [27] (formerly known as Pro/Mechanica) and StressCheck [32]. ANSYS [23] and Nastran [25] also have limited *p*-element capability, although it is not as widely used as their *h*-element approaches.

2.6 *K*-extraction method in both techniques

Three methods for extracting stress intensity factors from finite element solutions are presented. The virtual crack extension method is included because it was significant in the development of the domain integral method. The domain integral method and contour integral methods are also presented and have emerged as powerful approaches in the determination of three-dimensional stress intensity factors [28].

2.6.1 Virtual crack extension method

One method for calculating stress intensity factors is the virtual crack extension method [29]. Here the energy release rate G is calculated along the crack front. From G the stress intensity factor can be calculated for plane strain as:

$$K_I = \sqrt{\frac{E}{(1-\nu^2)} G} \qquad \textbf{Equation 9}$$

The virtual crack extension technique can be divided into two approaches [1]. The first is the stiffness derivative formulation. It is a precursor to the other contour integral methods, and is now considered outdated. The stiffness derivative formulation calculates the energy release rate G from its relationship to the finite element stiffness [30]. Another approach to the virtual crack extension method is the continuum approach. Rather than relying on the finite element stiffness and displacement matrices, this approach considers the energy release rate of a continuum. As such this approach is not limited to finite element methods.

The virtual crack extension method is not suitable for calculating K values for the separate modes under mixed mode loading [7]. Bakker concluded that the virtual crack

extension method of stress intensity factor calculation may require a finer mesh than other methods.

2.6.2 Domain integral method

The *h*-element code used in this study, Abaqus, uses the domain integral method to evaluate contour integrals. The method is robust in the sense that accurate contour integral estimates are usually obtained even with quite course meshes [31]. This is due to the fact that the integral is assessed over a domain of elements surrounding the crack, lessening the effect of errors in local solution parameters. A weighted mean of pointwise values within each domain is used, and thus the accuracy of the extracted values increases as the domain sizes are decreased [28]. In other words, as the through-thickness mesh density is increased the accuracy of the extracted values increases. Abaqus first calculates the energy release rate *J*, from which it then calculates the required *K* values.

Considering a two-dimensional problem, the domain integral approach uses a closed contour as shown in Figure 8. Here there is an outer integral Γ_1, an inner integral Γ_0, and integrals Γ_+ and Γ_- along the upper and lower crack faces.

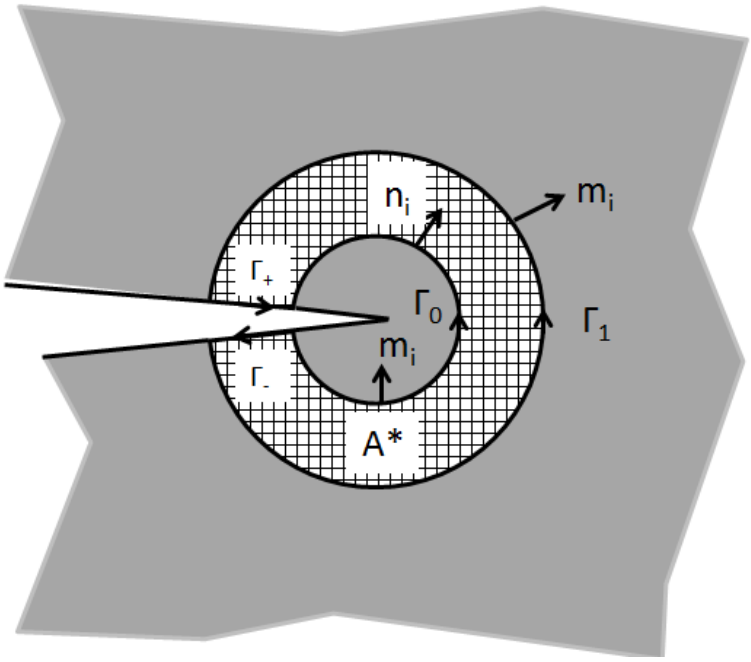

Figure 8: Two-dimensional domain integral [1]

In the absence of body forces, thermal strains, and crack-face tractions, the domain integral approach calculates J as follows [1]:

$$J = \int_{A*} \left[\sigma_{ij} \frac{\partial u_j}{\partial x_1} - w\delta_{1i} \right] \frac{\partial q}{\partial x_i} dA \qquad \textbf{Equation 10}$$

Here $A*$ is the area enclosed by the integral, q is an arbitrary but smooth function that is equal to unity on Γ_0 and zero on Γ_1, u_j is the crack-opening displacement, w is the strain energy density, and δ_{ij} is the Kronecker delta.

Rather than using an area integral, generalization of the domain integral to three dimensions involves using a volume integral. The approach is illustrated in Figure 9.

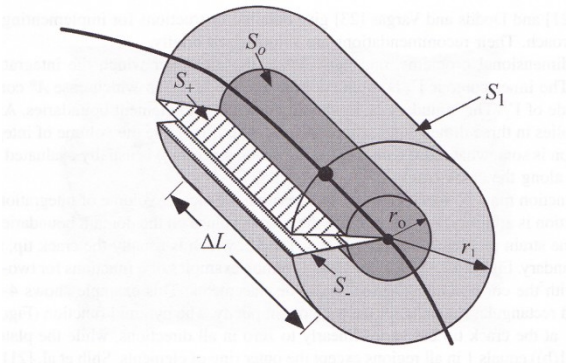

Figure 9: Three-dimensional domain integral [1]

The equation for this is [7]:

$$\bar{J}\Delta L = \int_{V*} \left\{ \left[\sigma_{ij} \frac{\partial u_j}{\partial x_1} - w\delta_{1i} \right] \frac{\partial q}{\partial x_i} + \left[\sigma_{ij} \frac{\partial \varepsilon_{ij}{}^p}{\partial x_1} - \frac{\partial w^p}{\partial x_1} - F_i \frac{\partial u_j}{\partial x_1} \right] q \right\} dV - \int_{S_+ + S_-} \sigma_{2j} \frac{\partial u_j}{\partial x_1} q d\Gamma \qquad \textbf{Equation 11}$$

Here V^* is the volume of the segment, ΔL is the length of the crack front segment, S_+ and S_- are the upper and lower crack faces, and F_i is the force vector. The superscript p denotes the plastic portions of work and strain. This equation calculates a weighted average of J over the crack front segment, and assumes a local coordinate system. The individual stress intensity factors can then be extracted using the following relationship:

$$J = \frac{1}{8\pi} K^T B^{-1} K \qquad \textbf{Equation 12}$$

where

$$K = [K_I, K_{II}, K_{III}]^T \qquad \textbf{Equation 13}$$

and *B* is called the pre-logarithmic energy factor matrix [31].

The domain integral approach is extremely versatile in that it is applicable to static, dynamic, elastic, plastic, and viscoelastic problems. It is relatively simple to implement numerically and is very efficient [1]. The domain integral method is usually implemented with the aid of structured meshes and special treatment of the crack front elements [28]. One drawback of the domain integral method is that the integral estimates may be inaccurate at the crack front ends. This can be compounded if the element quality near the crack ends is undesirable [31].

2.6.3 Contour integral method

StressCheck [32] uses the contour integral method to calculate Mode I and Mode II stress intensity factors. The contour integral method was originally proposed by Szabó and Babuška [33] in context of the *p*-element finite element method. For a planar solution, the Mode I stress intensity factor is calculated as follows:

$$K_I = \sqrt{2\pi} A_1 \qquad \textbf{Equation 14}$$

Here the *A* term is the first term of the asymptotic expansion of the solution in the neighborhood of the crack tip and is defined as follows:

$$A_1 = \int_{\Gamma} \left(W\, T_{FE} - u_{FE} T^{(W)} \right) ds$$

where *W* is an extraction function, T_{FE} is the traction vector along Γ computed from the finite element solution u_{FE}, and $T^{(W)}$ is the traction vector along Γ due to the extraction function [32].

Expanding along Γ,

$$T_{FE} = \begin{bmatrix} T_x \\ T_y \end{bmatrix}_{FE} = \begin{bmatrix} \sigma_x \cos\theta + \tau_{xy} \sin\theta \\ \tau_{xy} \cos\theta + \theta_y \sin\theta \end{bmatrix}_{FE} \quad \textbf{Equation 15}$$

and

$$u_{FE} = \begin{bmatrix} u_x \\ u_y \end{bmatrix}_{FE} \quad \textbf{Equation 16}$$

The terms due to the extraction function are

$$W = \frac{\rho^{-\frac{1}{2}}}{D}\{\psi\theta\}$$

$$T^W = -\frac{G\rho^{-\frac{3}{2}}}{D}\{\gamma\theta\} \quad \textbf{Equation 17}$$

Here *G* is the modulus of rigidity rather than the energy release rate, and *D* is given by:

$$D = \pi(2\kappa - 1) \quad \textbf{Equation 18}$$

For plane strain

$$\kappa = (3 - 4\nu) \quad \textbf{Equation 19}$$

and for plane stress

$$\kappa = \frac{3 - \nu}{1 + \nu} \quad \textbf{Equation 20}$$

Also

$$\{\psi(\theta)\} = \begin{bmatrix} \left(\kappa - \frac{1}{2}\right)\cos\frac{\theta}{2} - \frac{1}{2}\cos\frac{3\theta}{2} \\ \left(\kappa + \frac{1}{2}\right)\sin\frac{\theta}{2} - \frac{1}{2}\sin\frac{3\theta}{2} \end{bmatrix}$$

$$\{\gamma(\theta)\} \qquad \textbf{Equation 21}$$

$$= \begin{bmatrix} \left(\frac{3}{2}\cos\frac{\theta}{2} + \frac{1}{2}\cos\frac{5\theta}{2}\right)\cos\theta + \left(\frac{1}{2}\sin\frac{5\theta}{2} - \frac{1}{2}\sin\frac{\theta}{2}\right)\sin\theta \\ \left(\frac{1}{2}\sin\frac{5\theta}{2} - \frac{1}{2}\sin\frac{\theta}{2}\right)\cos\theta + \left(\frac{5}{2}\cos\frac{\theta}{2} - \frac{1}{2}\cos\frac{5\theta}{2}\right)\sin\theta \end{bmatrix}$$

In order to expand this into three dimensions, the following changes are made:

$$\gamma = \left|\frac{\sigma_z}{\sigma_x + \sigma_y}\right|$$

$$\kappa = \begin{Bmatrix} \kappa_1 \ \ if \ \ (\gamma > \gamma_1) \\ \kappa(\gamma) \ \ if \ (\gamma < \gamma_1) \end{Bmatrix} \qquad \textbf{Equation 22}$$

where

$$\gamma_1 = 0.1$$

$$\kappa(\gamma) = \kappa_1 + (\kappa_2 + \kappa_1)\left(\frac{2\gamma}{\gamma_1} + 1\right)\left(1 - \frac{\gamma}{\gamma_1}\right)^2 \qquad \textbf{Equation 23}$$

The contour integral method is described as being super-convergent, in that the errors in stress intensity factors converge to zero much faster than the error in strain energy as the number of degrees of freedom increase [34] [35]. Wen [36] states that the contour integral method leads to increased accuracy in stress intensity factor extraction, even with course meshes. Another advantage of this approach is that it can extract stress intensity factors directly for mixed mode problems [35].

2.7 Experimental methods for determining the Stress Intensity Factor

A vast amount of work has been done on the development of analytical methods for determining stress intensity factors in elastic solids. Experimental methods are also needed to compliment such analytical methods, providing guidance for future analytical methods and verification of current approaches [37]. A few experimental methods are highlighted here.

2.7.1 Two-dimensional

Several experimental methods exist for determining K_I for through-cracked, thin planar specimens. K_I can be determined by using three strain gages in the near field region on the plate's surface. K_I is calculated using the relationship

$$K_I = A_0\sqrt{2\pi} \qquad \textbf{Equation 24}$$

where A_0 is an unknown coefficient which can be solved with data from the strain gage readings. The strain gage approach can be reduced to a single gage through precise placement of that single gage, as shown in Figure 10.

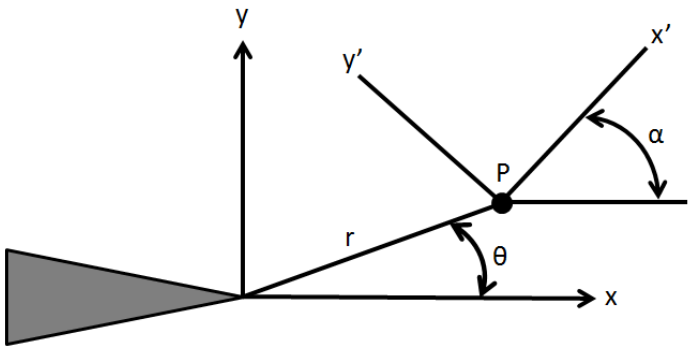

Figure 10: Placement of single strain gage for K_I determination [13]

The gage is placed at P at an angle θ to the crack plane, and its axis x' is oriented at an angle α to the crack plane. The necessary angles θ and α depend on the material's Poisson's ratio. The equation relating K_I to the strain reading $\varepsilon_{X'X'}$ is [13]:

$$2\mu\varepsilon_{x'x'} = \frac{K_I}{\sqrt{2\pi r}}\left[k\cos\frac{\theta}{2} - \frac{1}{2}\sin\theta\sin\frac{3\theta}{2}\cos 2\alpha + \frac{1}{2}\sin\theta\cos\frac{3\theta}{2}\sin 2\alpha\right] \quad \textbf{Equation 25}$$

The remaining methods discussed here for determining K_I in two-dimensional bodies are optical in nature. Photoelastic methods are preferred as they provide a rich field of data near the crack tip which can be used for accurate K_I determination. In photoelasticity, either a special model is built from a photoelastic material, often a polymer, or a photoelastic coating is applied to the specimen itself. The model or specimen is placed in a polariscope, which is an optical instrument that employs polarized light in its operation. The specimen is then loaded and the resulting fringe pattern is recorded and interpreted. Irwin, credited for developing the concept of the stress intensity factor, also developed a method for determining K_I from the geometric characteristics of the fringe loops near the crack tip. Irwin's approach is known as the apogee method [13].

Caustics is an experimental method which transforms a stress singularity into an optical singularity. Typically a laser is used to project a coherent light beam on a cracked specimen in the vicinity of the crack tip [38]. If the specimen is transparent the light is transmitted through it. Opaque specimens can also be used if one surface of the specimen is mirrored [13]. The specimen is subjected to an applied load, which causes an abrupt

change in thickness, Δh, in the area of the stress singularity [38]. This change in thickness is characterized by the following equation [13]:

$$\Delta h = -\frac{h\nu}{E}(\sigma_{XX} + \sigma_{YY}) \qquad \textbf{Equation 26}$$

where h is the specimen thickness. The change in thickness causes a scattering of the reflected light, which when projected onto a reference screen is concentrated along a curve. This curve is called a caustic [38]. Stress intensity factors can then be determined from the caustics from the following equation [13]:

$$K_I = 0.0934\frac{D^{3/2}}{z_0 C_1 h} \qquad \textbf{Equation 27}$$

where D is the diameter of the caustic, z_0 is the distance from the specimen to the reference screen, and C_1 is an optical constant. Caustics can also be used to provide information about the triaxiality in the crack region [38]. Caustics has proven to be one of the most successful experimental methods to determine fracture properties due to its sensitivity to strain gradients, simplicity [39], and efficiency [40].

The coherent gradient sensing method (CGS) measures in-plane stress fields in planar solids [43]. CGS measures the same mechanical fields as caustic approaches, but differs in that it provides full-field information. The use of CGS in experimental fracture mechanics employs a laser as a light source, and a camera as a recording device. Depending on whether the specimen is transparent or not, light waves are either transmitted through or reflected off of the specimen. These light waves then pass through two parallel gratings, which diffract the light. These gratings typically consist of glass planes with chrome depositions, commonly referred to as Ronchi gratings [13]. The light then travels through a filtering lens, and a filtering plane. An aperture on the filter plane

allows only the necessary diffracted light to pass on to the camera, where the resulting interferograms are recorded. The interferograms are then used to determine surface deformations in the area of the crack plane [41]. The displacement information is then used to calculate stress intensity factors.

Digital image correlation is an optical method which has been used to extract stress intensity factors of thin planar specimens. The basis of the method is that an optical image of the specimen is recorded at some initial state, and then a second image is recorded after a deforming load is placed on the specimen. The specimens are often enhanced by depositing a pattern of dots on the surfaces to be imaged, usually with spray paint. For each image the light intensity of each pixel is determined. A correlation between the two images is done to quantify the displacement field. The correlation involves determining unique features of the plate, in the form of clusters of pixels with unique shapes and light intensities. For its application in fracture mechanics, digital image correlation is used to determine the displacement field around the crack tip [37]. Chu [42] presents the mathematical means for solving stress intensity factors from the displacement field.

2.7.2 Three-dimensional

Much of the recent experimental research in linear elastic fracture mechanics has been focused on development of stress intensity factor solutions for three-dimensional cracked-body problems [16]. The following methods are used for three-dimensional fracture analysis, but may also be used for two-dimensional cases.

Moiré techniques are those where displacements are measured using two sets of gridding placed on the surface of model; one set is adhered to the surface, whereas the

other set is not and acts as a reference to measure relative displacements [43]. The displacement field is related to the moiré fringe orders N by [13]:

$$u, v = Np \qquad \textbf{Equation 28}$$

where p is the pitch of the master grating. This information is then used to obtain K_I.

Dhar et al [44] used an experimental method based on the moiré technique to determine Mode I stress intensity factors in polycarbonate. They called their method the multiple embedded grid moiré technique, because the specimens were made of multiple layers of polycarbonate bonded together with gridding between the layers. The grids are used to measure the crack opening displacement with high resolution photography, which is then used to calculate stress intensity factors at different locations through the specimen thickness. Their findings concluded that the stress intensity factor was higher on the midplane than on the specimen surfaces. Dhar claims that at the time of their paper (1989), several researchers were trying to solve the three-dimensional stress intensity factor analytically, but that only experimental methods have been successful in that endeavor.

A frozen-stress photoelastic determination of the *SIF* for a through-cracked semi-infinite plate can be performed as follows. A stress-freezing photoelastic material, typically a thermosetting polymer [45], is cast into through-thickness sections and starter cracks are introduced [16]. These cracks can either be artificial, which are machined into the material, or natural cracks. Natural cracks are formed by impacting the material surface with a sharp blade, and then cyclically loading the material which causes the cracks to grow until the desired crack length is achieved. The cracked sections are then glued together. The model is subjected to a stress-freezing cycle under load in an oven at

a temperature higher than the material's glass-transition temperature, and then allowed to cool slowly to room temperature. Thin through-thickness slices are cut from the model and analyzed with a polariscope to identify fringes [16]. The term stress-freezing comes from the fact that these materials retain the strain and birefringence even when the load is removed and the model is cut into slices. Constitutive equations are then used to determine the stress fields in the slices. From these stress fields the stress intensity factors can then be determined [45]. Common materials used for frozen-stress photoelastic methods have Poisson's ratios of approximately 0.5, as compared to the Poisson's ratio of most engineering materials of about 0.3. Because of this difference, experimental results using these methods tend to overestimate the *SIF* in common engineering materials by about five percent [16]. The frozen-stress method has seen limited use in the past due to the time and therefore expense needed in its use, but is experiencing a gain in recent years. Improvements in material selection, slicing methods, and polariscopes are credited for the increased use of stress-freezing photoelasticity [45]. Epoxies have proven to be a nearly ideal stress-freezing material due to their castability, machinability, optical properties, and linearity in optical and mechanical properties [46].

Dhar [44] lists two additional experimental techniques that have been used by other researchers for this same investigation:

1. Crack opening interferometry measuring the separation of the crack faces by observing the destructive interference of light reflected by the two crack faces
2. Scattered light speckle interferometry which measures the change in displacements on any plane in a transparent model through the use of coincident coherent sheets of light traveling in opposite directions

3. Finite element analysis of crack geometries

3.1 Model

A series of finite element analysis studies were performed using conventional *h*-element as well as *p*-element methods, using both planar and three-dimensional models. For these studies the material was modeled as linear steel with the properties shown in Table 3.

Table 3: Steel properties used in analyses

Steel	
Modulus of elasticity	205 GPa
Poisson's ratio	0.3

The basic model is that of a center-cracked plate with the dimensions shown in Figure 11, subjected to a remote tensile load along the long axis. When subjected to a 200 MPa remote stress, the basic closed-form Mode I stress intensity factor for this geometry is 26.145 MPa·$m^{1/2}$, accounting for the finite width. This can be obtained by using the geometric and loading parameters defined in Equation 7.

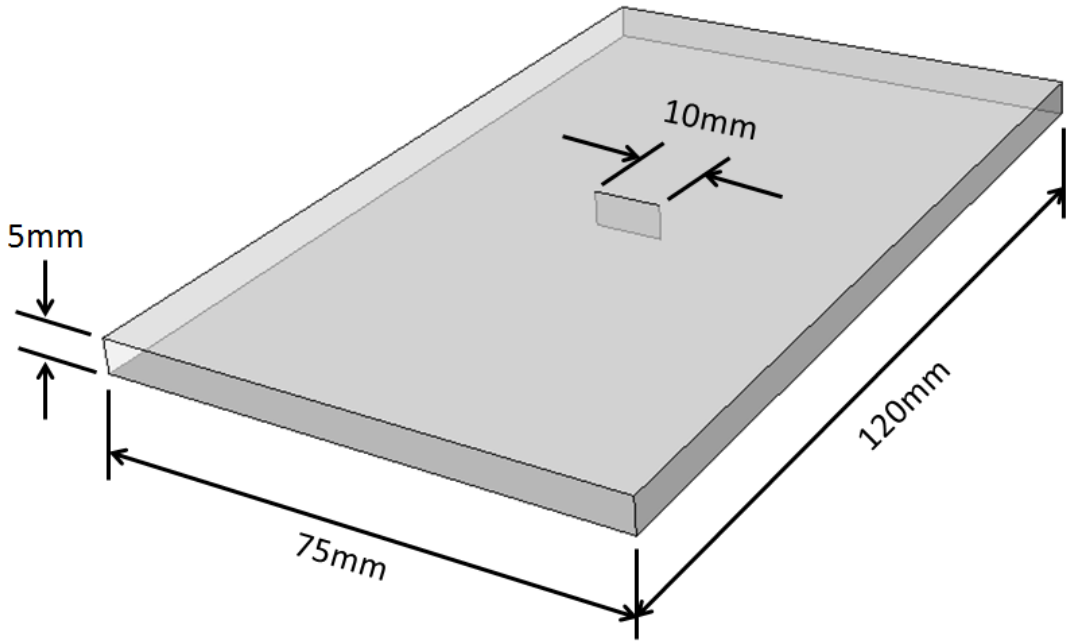

Figure 11: Baseline model dimensions (Note crack is a through-thickness crack)

3.2 Planar analysis

Planar finite element models analogous to the three-dimensional models were developed to quantify the potential error in making planar assumptions for determining the stress intensity factors. In the following section, planar models in the *h*-element and *p*-element approaches are examined.

A two-dimensional Abaqus model was built which closely matches the topographical mesh used in the three-dimensional studies, as shown in Figure 12. The model consists of 4,978 quadratic reduced integration elements, type S8R. The shell thickness is 5.0 millimeters, and the same 200 MPa remote load was applied.

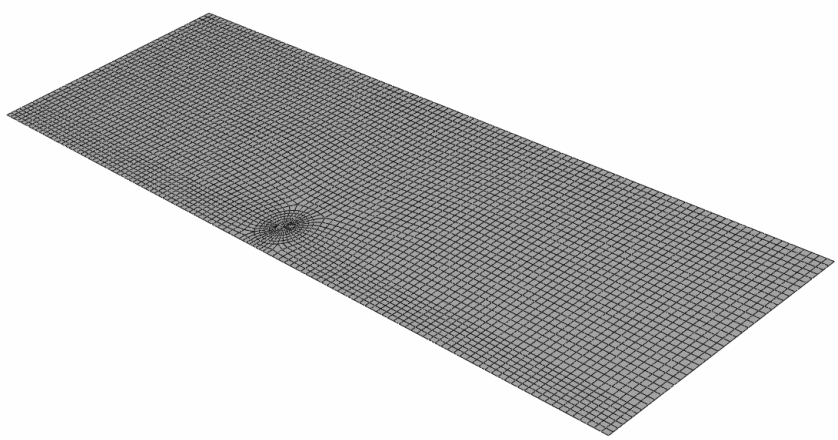

Figure 12: Abaqus planar model for center cracked specimen

The computed K_I value, averaged for contours three through five, was found to be 25.359 MPa·m$^{1/2}$.

A similar Abaqus model was also built to assess the effect of using two-dimensional plane strain and plane stress elements, type CPE8 and CPS8 elements respectively. The difference in computed K_I values was insignificant, with both plane strain and plane stress elements reporting a K_I of 25.356 MPa·m$^{1/2}$. This slight difference may be attributable to minor differences in the two meshes.

A two-dimensional StressCheck model was built which closely matches the topographical mesh used in the three-dimensional studies, as shown in Figure 13. The model consists of 276 elements. The shell thickness is 5.0 millimeters, and the same 200 MPa remote load was applied. The computed K_I value was found to be 25.352 MPa·m$^{1/2}$. Both plane strain and plane stress solutions were computed from the same model, and both produced the same K_I value.

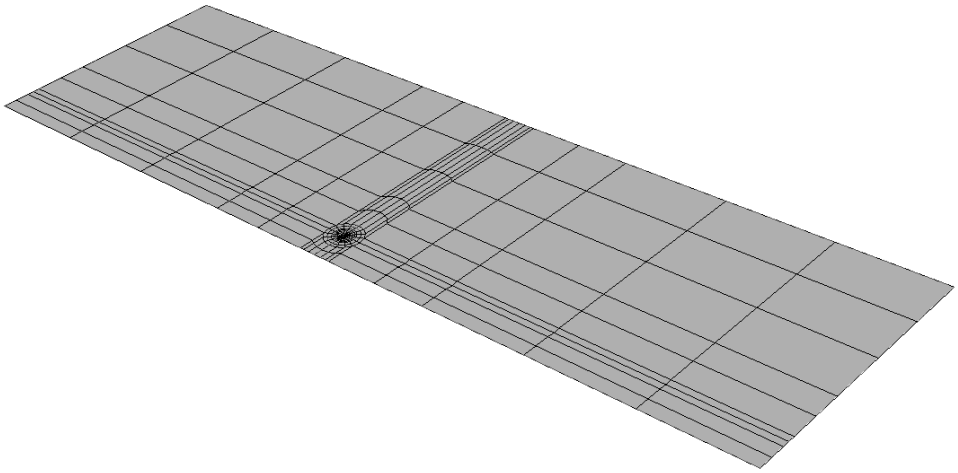

Figure 13: StressCheck planar model

3.3 Three-dimensional analysis

3.3.1 *H*-element analysis

The *h*-element analysis was performed using Abaqus/Standard [24]. Two planes of symmetry were used, with one perpendicular to the crack plane and another perpendicular to the thickness, as shown in Figure 14.

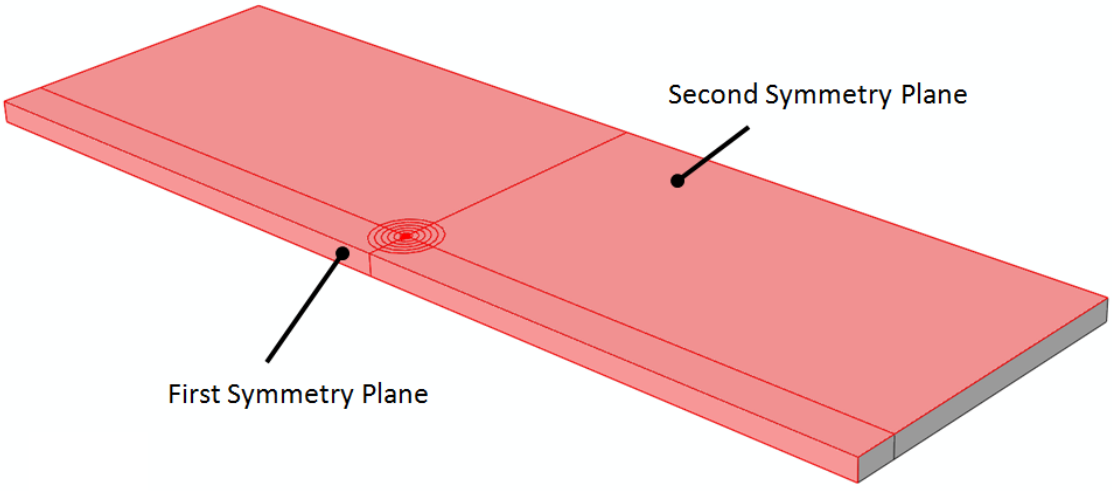

Figure 14: *H*-element geometry model with two planes of symmetry

Within Abaqus/CAE a seam crack is introduced by defining the faces which represent the crack plane, followed by defining the crack edge, as shown in Figure 15.

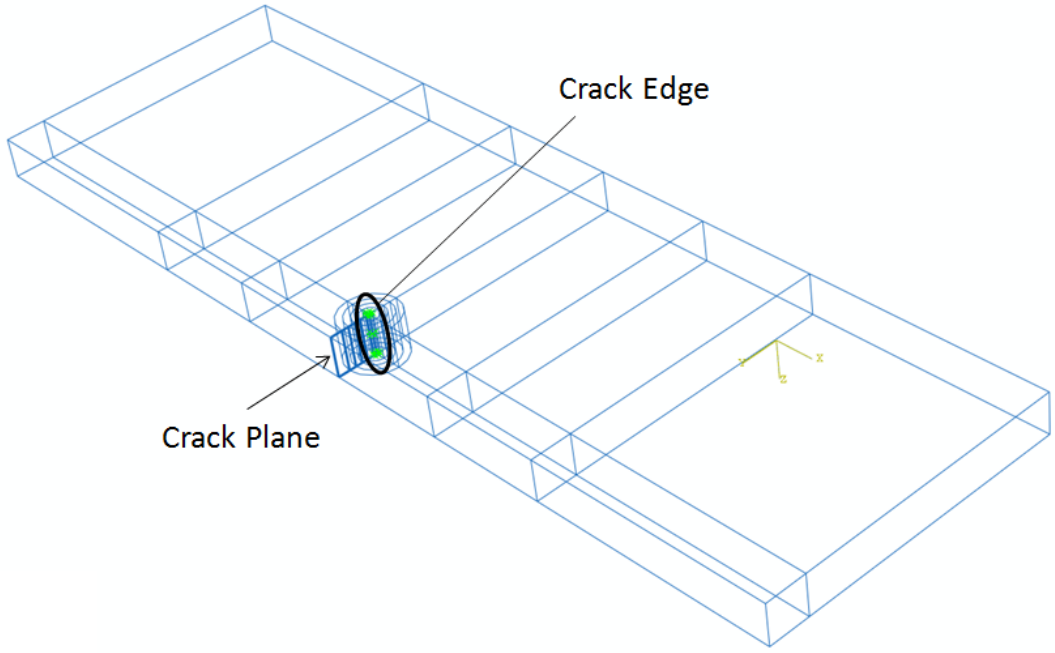

Figure 15: Crack definition in Abaqus/CAE (in quarter model)

In order to accurately compute the contour integral, a singularity is artificially introduced at the crack front. This is done by using degenerated quadratic elements, such that the topology of the element is collapsed from a quadrilateral shape to a triangular shape. Further, the midside nodes on the element sides which are then pointed at the crack edge are moved to distances one-quarter of the element's length from the crack edge. This results in a singularity of $r^{-1/2}$ for the stresses in this zone. This is shown graphically in Figure 16.

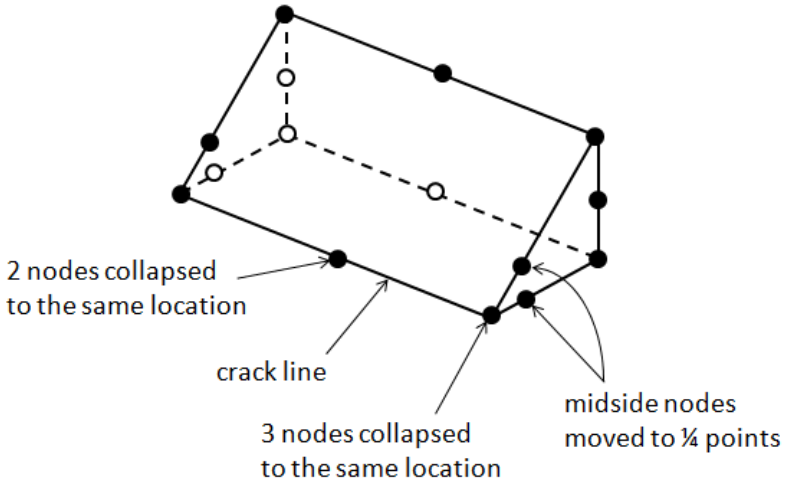

Figure 16: Introduction of singularity in *h*-element model

The mesh, shown in Figure 17, consists of 18,700 second-order reduced integration hexahedral solid elements, type C3D20R. Seven concentric rings of elements were used around the crack edge for the purpose of computation of the contour integral which is subsequently used to determine *K*.

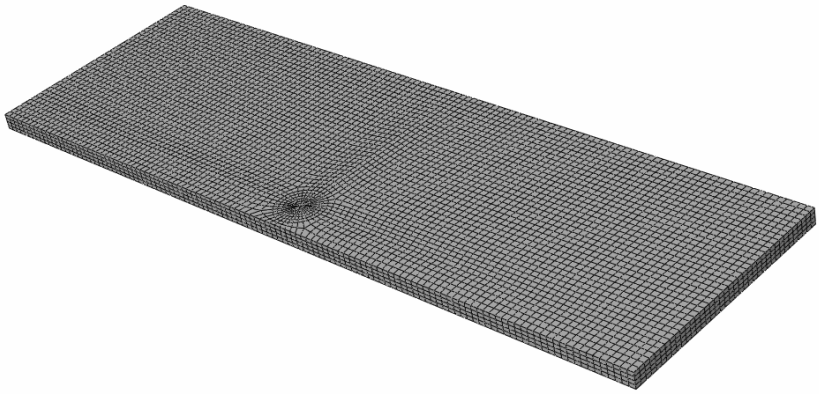

Figure 17: *H*-element finite element mesh

A 200 MPa remote traction load was applied, equivalent to 37,500 N on the half-symmetry model, or 75,000 N on the full model. The deformed shape is shown in Figure 18 with a contour of the longitudinal stress. The deformed shape is scaled +100x.

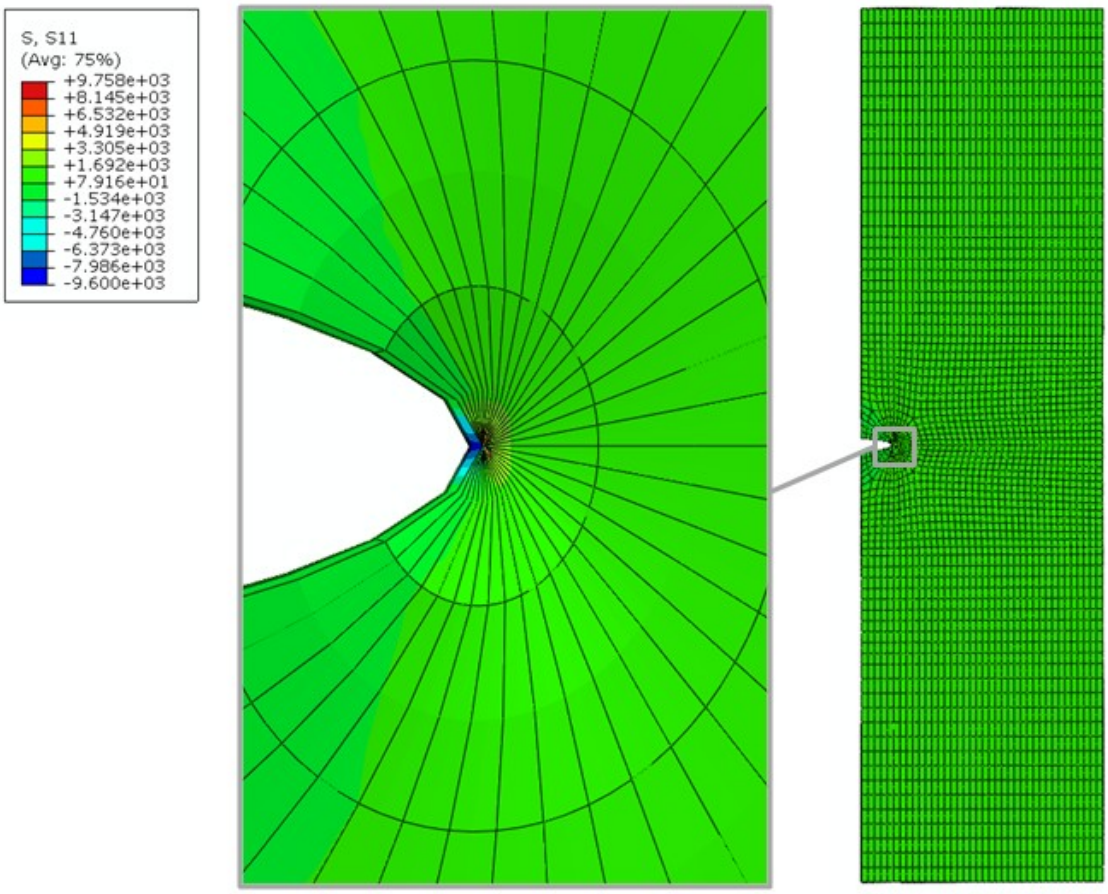

Figure 18: *H*-element deformed plot showing the longitudinal stress contour

Calculating K_I directly using the contour integral approach

Six contour integral outputs were determined from the results. The raw output for all six contours is shown in Figure 19. It is generally considered good practice to consider the average of a series of contours just outside the crack tip. The results from averaging contours three through five are shown in Figure 20, and can be compared to the closed-form solution of 26.145 MPa·m$^{1/2}$. The Mode I stress intensity factor is computed by first extracting J_I along the crack edge. Then K_I is calculated using both plane stress and plane strain assumptions. This is shown in Figure 21. Results from Figure 20 are included for comparison.

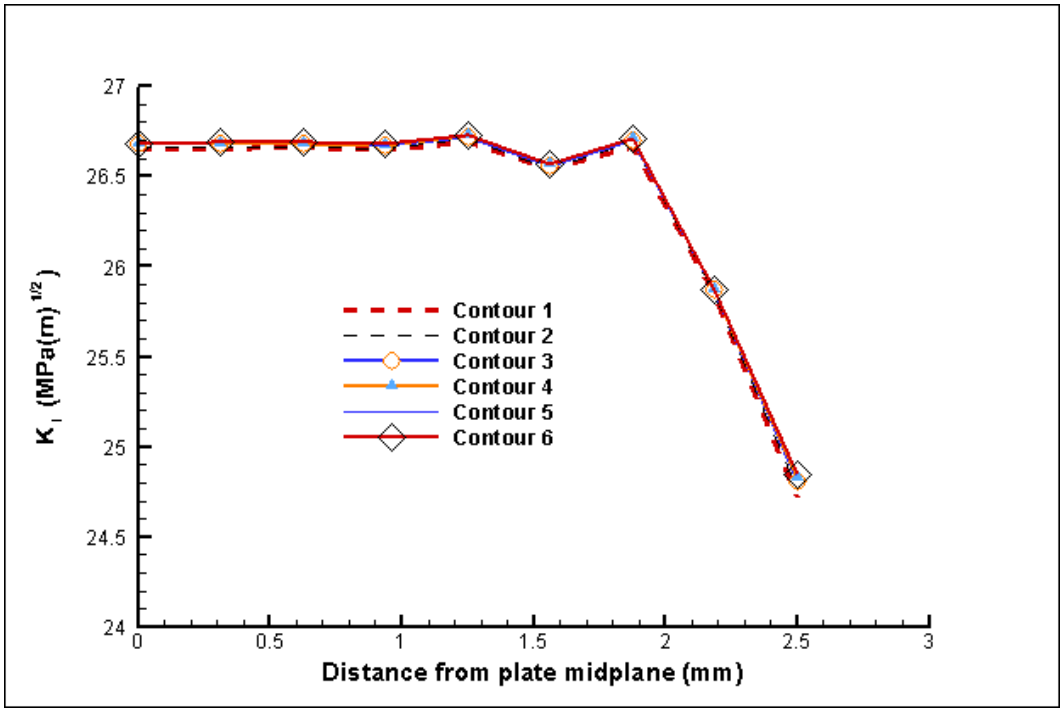

Figure 19: K_I output for all six contour integrals

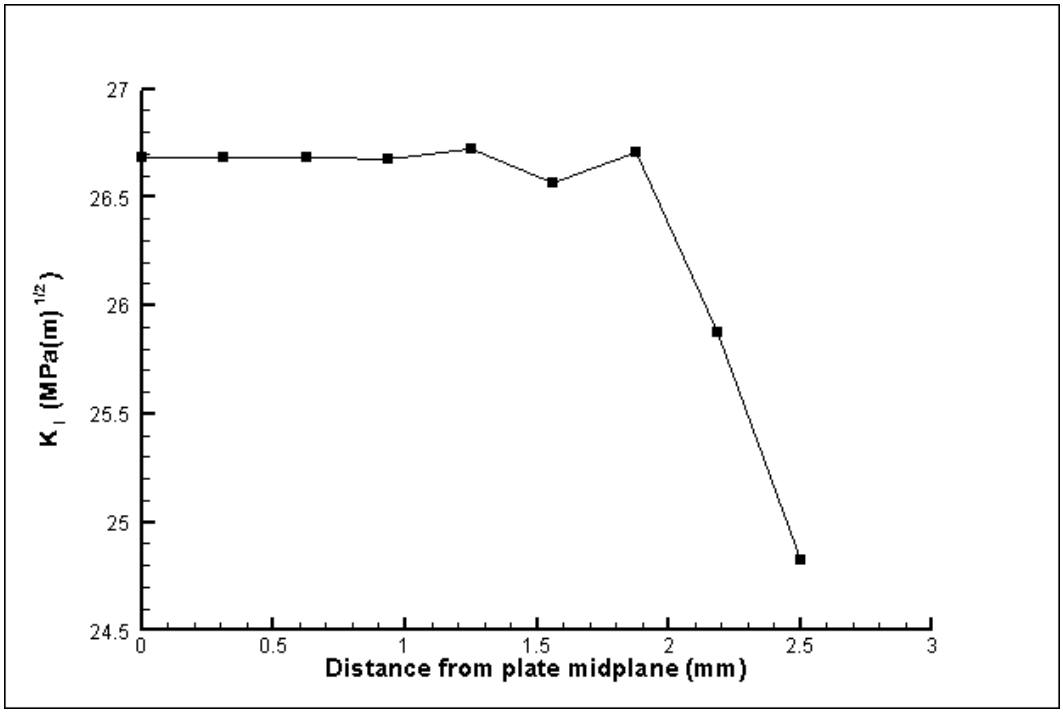

Figure 20: Average of contours three through five

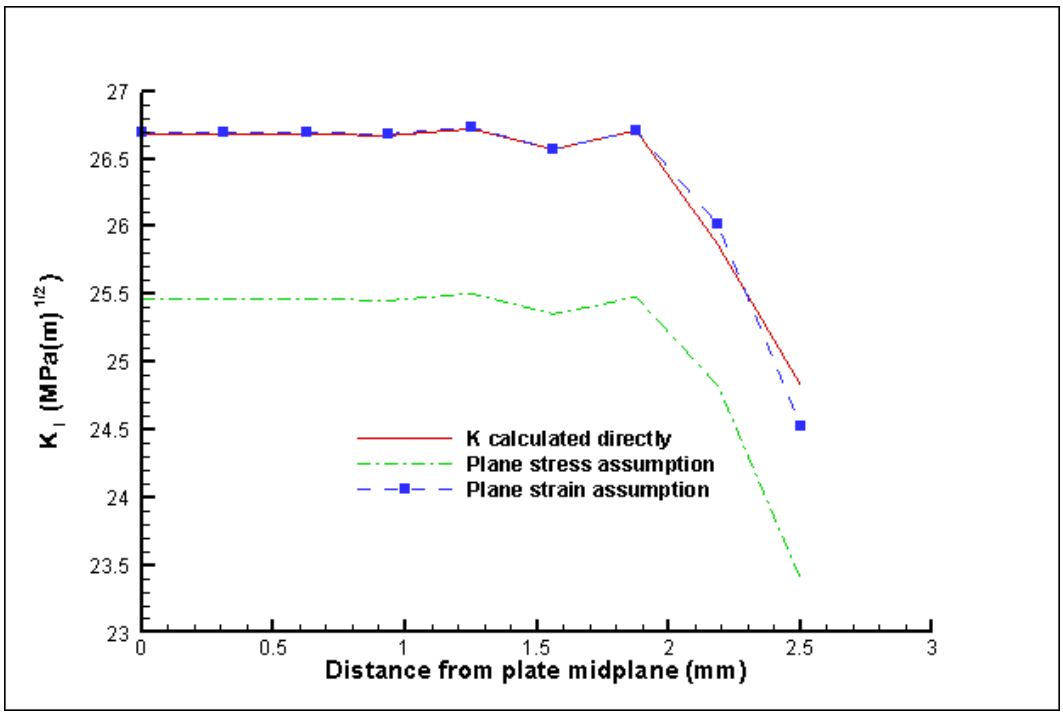

Figure 21: Comparison of *K* calculation methods for plane strain and plane stress assumptions

It can be seen that the K_I values calculated directly by the *h*-method match closely to the K_I values calculated from *J*, assuming plane strain. This is consistent with the findings of Bakker [7] that demonstrated a plane strain state near the crack front.

3.3.2 *P*-element analysis

The *p*-element models were developed using two planes of symmetry: one through the thickness and one perpendicular to the crack plane. This was done for computational efficiency. In order to introduce the crack into the model, the mesh is first constructed with a visible gap along the crack plane, as shown in Figure 22. Once the mesh is completed, the crack is closed by projecting the nodes on both sides of the crack plane so that they are coincident with the nodes on the other side of the crack plane. The completed mesh contains 1200 elements, and is shown in Figure 23. There are 6 rings of elements around the crack tip, as shown in Figure 24. There are fewer elements in the *p*-

element mesh as compared to the *h*-element mesh, both through the thickness and radially around the crack tip. This is typical of *p*-element meshes since the *p*-method involves raising the polynomial order of the elements to achieve mesh convergence rather than increasing the element density.

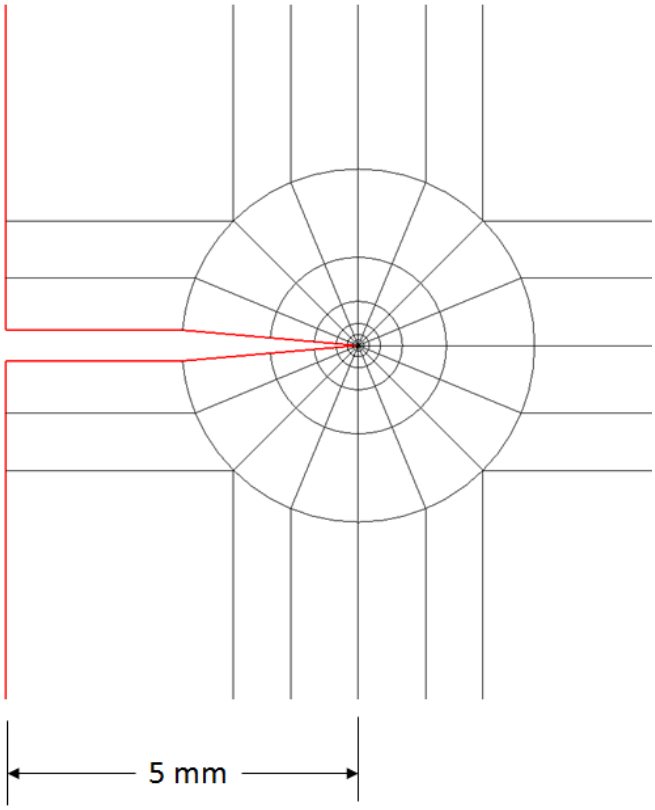

Figure 22: Introduction of crack into *p*-element mesh

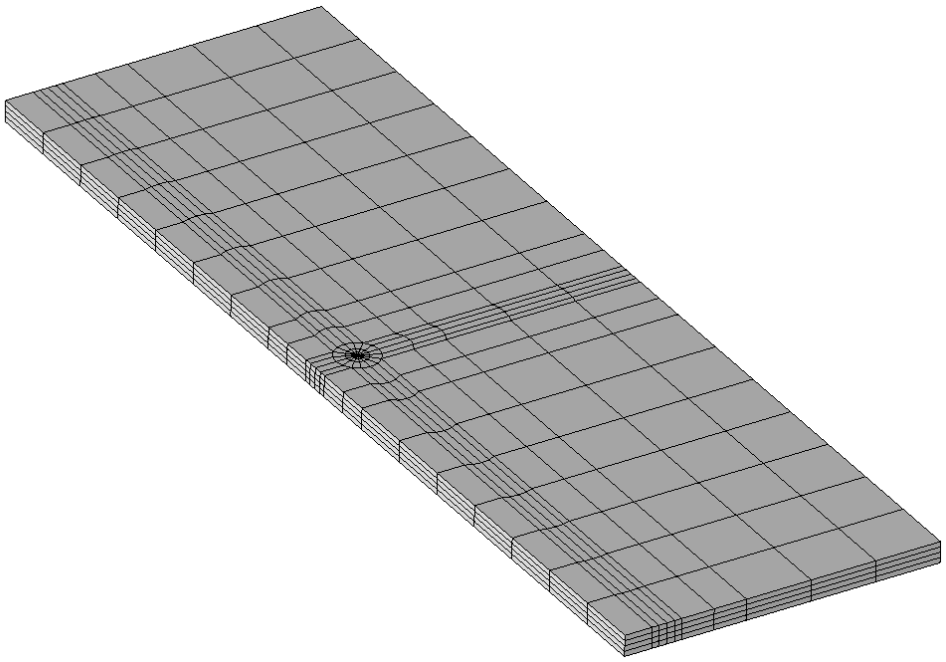

Figure 23: Completed *p*-element mesh

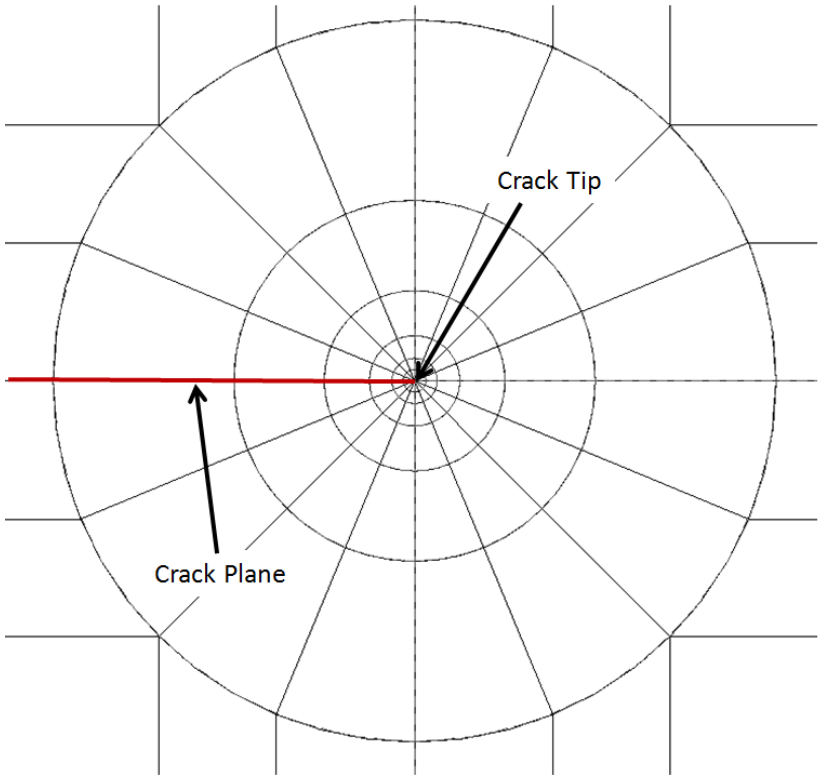

Figure 24: *P*-element mesh refinement around crack tip

A 200 MPa remote traction load was applied, as indicated by the arrows in Figure 25. This is equivalent to 18,750 N on the quarter-symmetry model, or 75,000 N on the full model. Two faces (shown in blue) were constrained with normal (symmetry) constraints, and a third face was constrained in the longitudinal direction, also shown in Figure 25.

The deformed shape is shown in Figure 26 with a contour of the longitudinal stress. The deformed shape shown has been scaled +100x. The Mode I stress intensity factor is extracted along the crack edge and plotted as a function of the distance from the plate centerline, shown in Figure 27. These values can be compared to the closed-form solution of 26.145 MPa·m$^{1/2}$, calculated using Equation 7. The K_I values determined by this approach differ from the *h*-element in that they are lower at the midplane and increase toward the free surface.

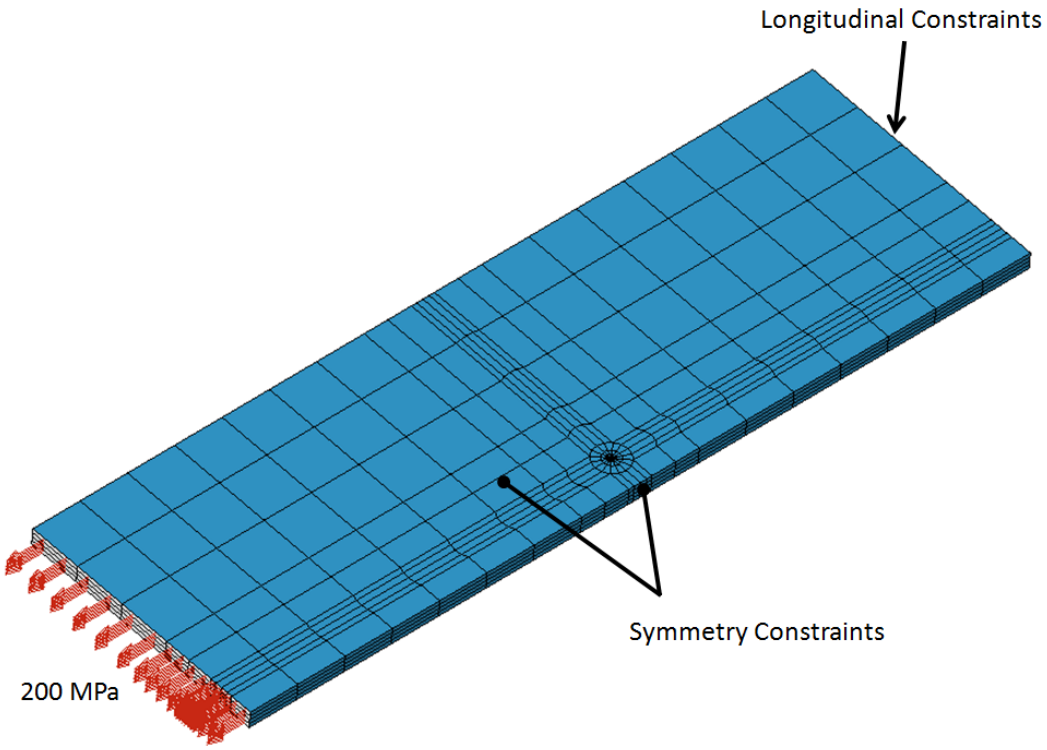

Figure 25: *P*-element model loads and boundary conditions

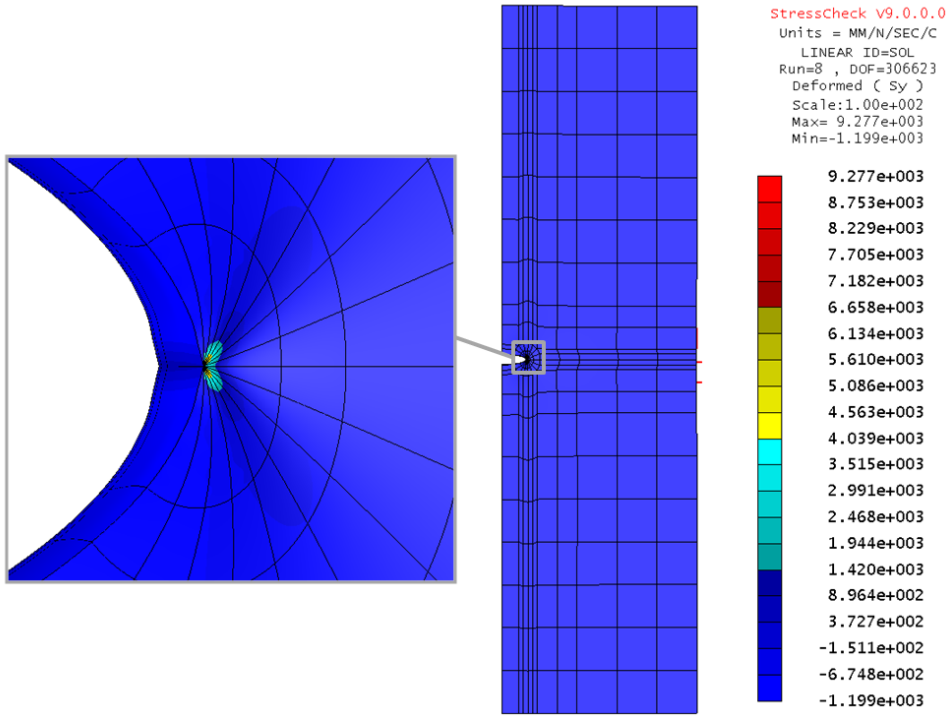

Figure 26: *P*-element deformed plot showing the longitudinal stress contour

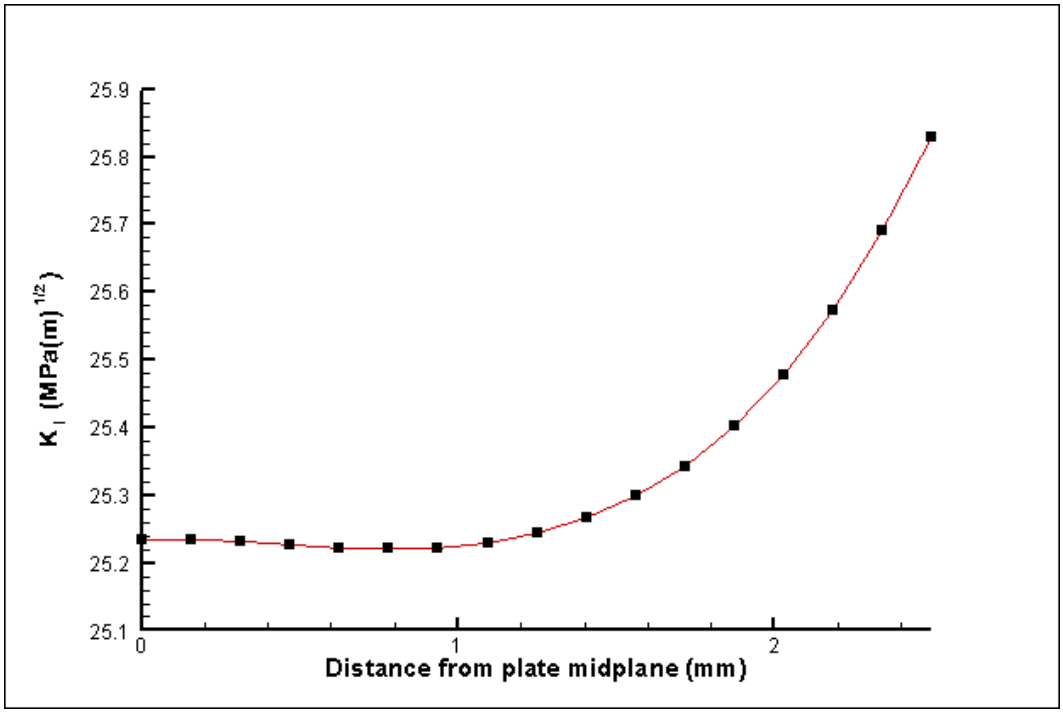

Figure 27: *P*-element Mode I stress intensity factors vs. distance from plate centerline

Figure 28 shows the rate of convergence of the three-dimensional *p*-element solution in terms of energy norm. The error in energy norm is similar to the root-mean-square measure of error in stress. In order to extract a converged stress intensity factor it is recommended to have an error in energy norm less than five percent [32]. As stated in Section 2.6.3, the error in stress intensity factor extraction converges much faster than the error in energy norm.

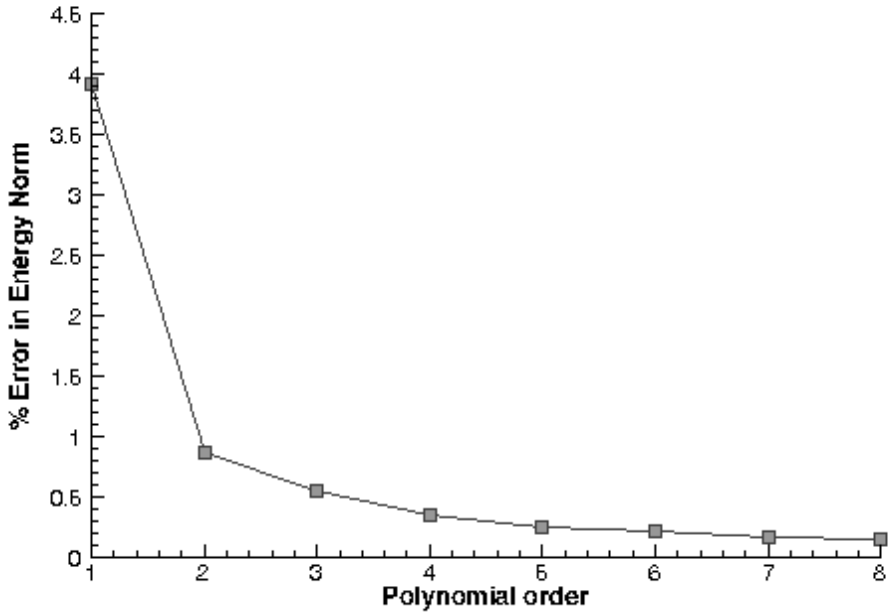

Figure 28: Convergence of 3D *p*-element solution

Calculating K_I from J_I

The Mode I stress intensity factor is computed by first extracting J_I along the crack edge. K_I is then calculated using both plane stress and plane strain assumptions. This is shown in Figure 29. The K_I values for the *p*-element method which are calculated from *J* values match the trend of those found in the literature review and those obtained

from the *h*-method. The K_I values here are highest at the midplane and decrease toward the plate's free surface.

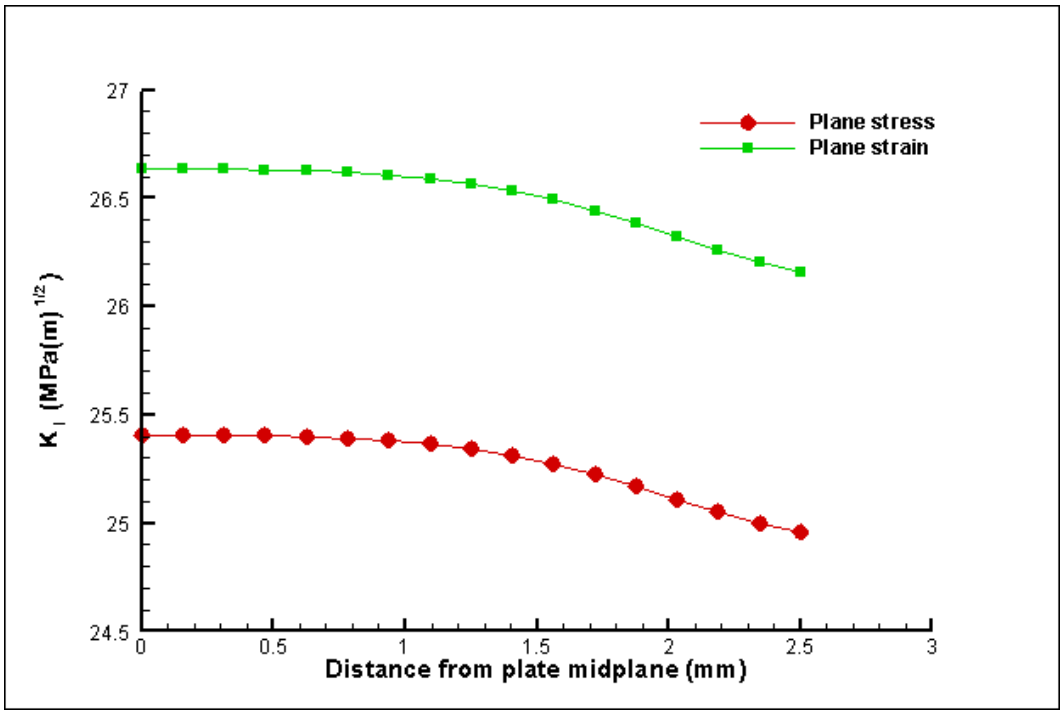

Figure 29: *P*-element K_I calculated from J_I

3.4 Mesh density study

In order to assure the through-thickness behavior is captured correctly, refined models were made for both *h*- and *p*-element models. The same topological density was used, but both models had their through-thickness densities doubled.

3.4.1 *H*-element mesh sensitivity

Several models were compared to study the effects of the mesh density on the results. The *h*-element model was changed from four elements to eight elements through the thickness, going from 18,700 to 37,400 total elements. The two mesh densities are compared in Figure 30. The results, shown in Figure 31, show less through-thickness

oscillation of K_I for the refined model compared to the baseline model. Based on the above results a subsequent through-thickness mesh refinement was done. The density was increased from eight to twelve elements through the thickness, for a total of 56,100 elements. The results are shown in Figure 32. The new results, labeled "second refinement" in Figure 32, show a marked improvement in smoothness compared to the previous results (labeled "first refinement") for the region away from the plate's midplane. Near the midplane the two sets of results are nearly identical. Table 4 summarizes the three different meshes.

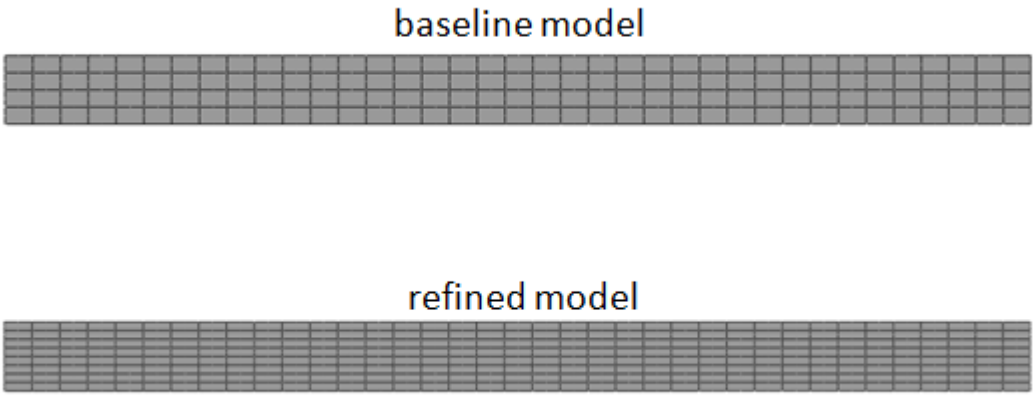

Figure 30: Comparison of *h*-element through-thickness mesh densities

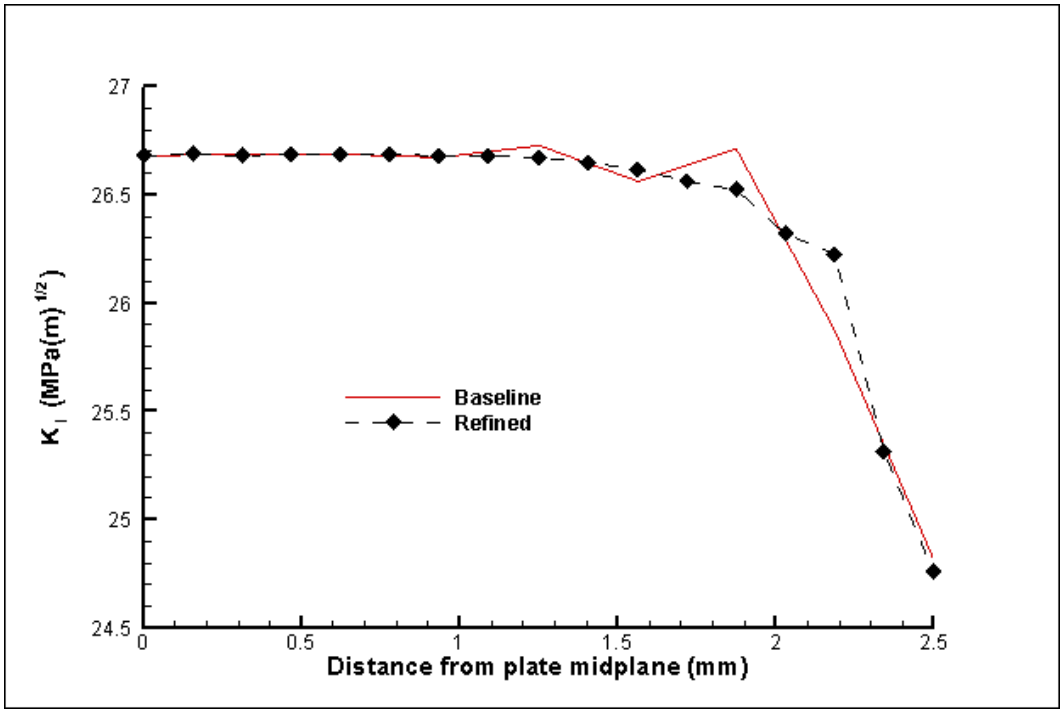

Figure 31: Effect of *h*-element though-thickness mesh density on K_I calculation

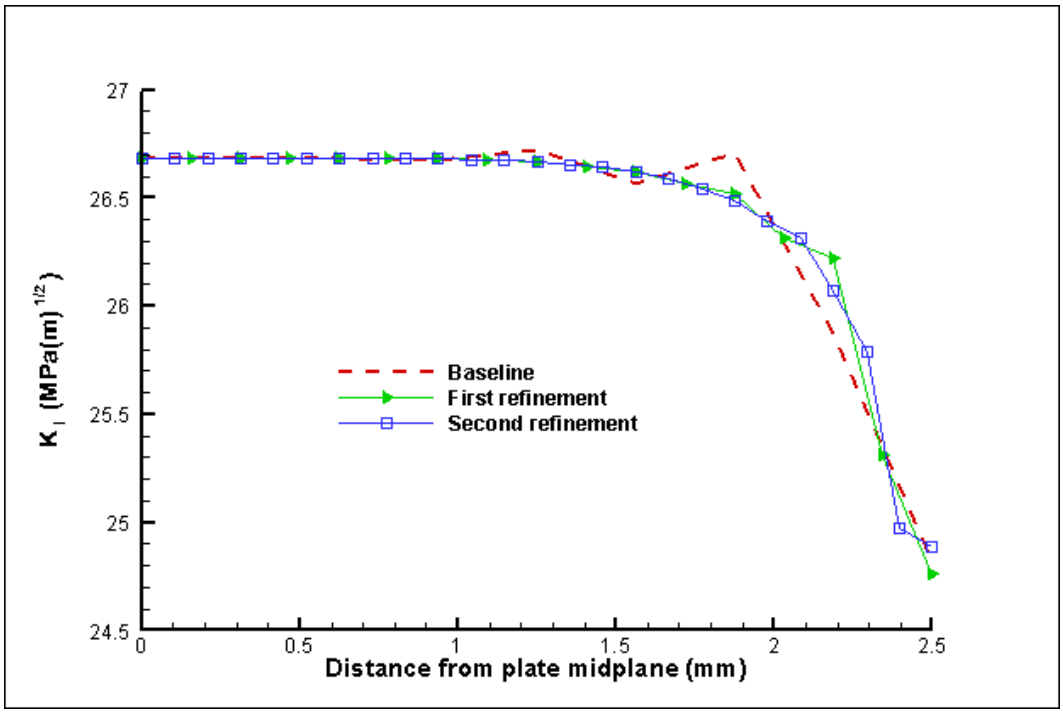

Figure 32: Further through-thickness refinement of the *h*-element model

Table 4: *H*-element mesh densities

Configuration	Number of Elements	Number of Elements Through the Thickness	Mesh Bias
Baseline	18,700	4	none
First Refinement	37,400	8	none
Second Refinement	56,100	12	none

3.4.2 *P*-element mesh sensitivity

The *p*-element model was changed from four elements to eight elements through the thickness, and 1200 to 2400 total elements. The two meshes are compared in Figure 33. Based on previous results, the *p*-element mesh study was done using K_I values calculated from *J* values. The results, shown in Figure 34, show there is no significant change in through-thickness Mode I stress intensity factor calculation between the two models. The denser model was used for subsequent investigations.

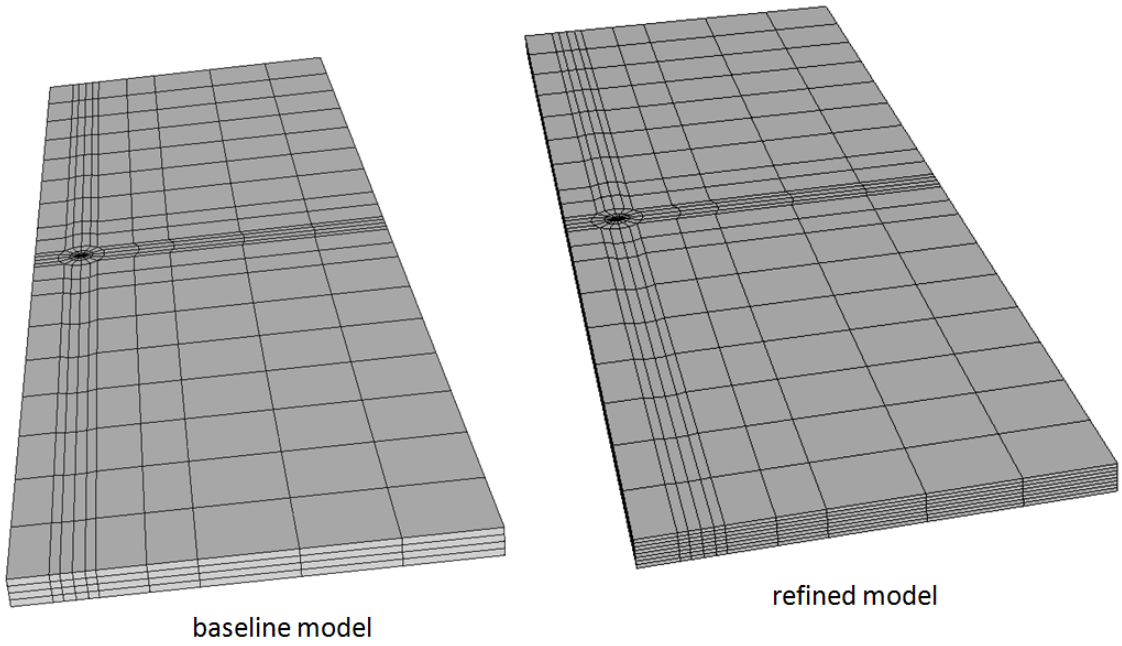

Figure 33: Baseline and refined *p*-element models

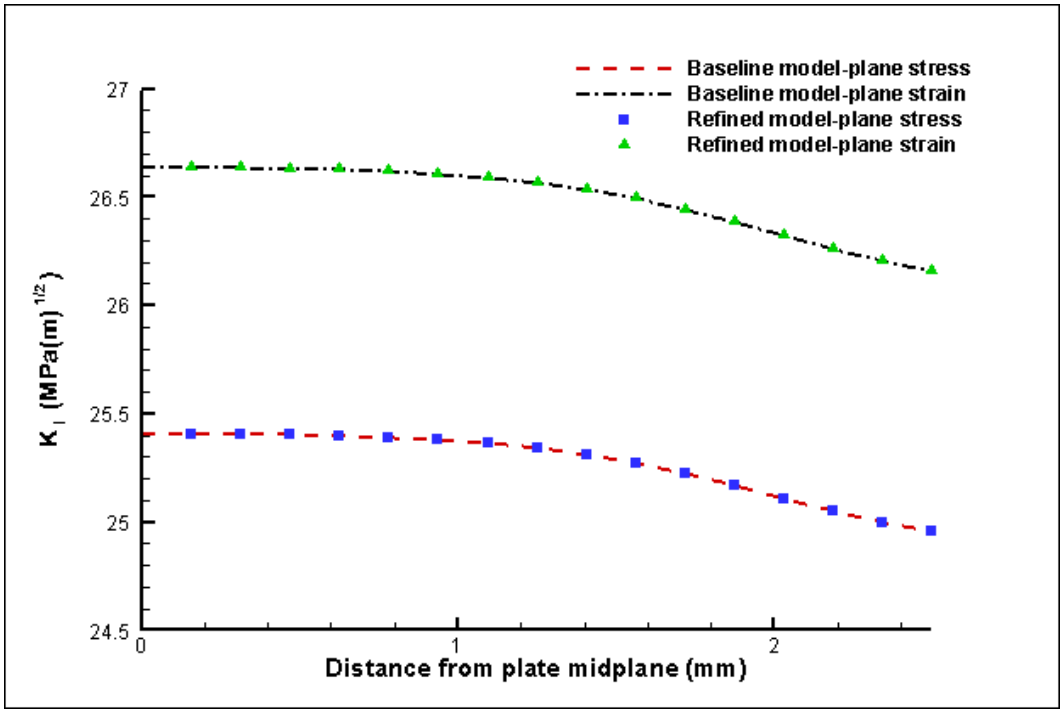

Figure 34: Effect of *p*-element through-thickness mesh density on K_I calculation

3.4.3 Comparing refined *p*-element and *h*-element results

Figure 35 shows the comparison of calculated K_I values for both finite element methods. The *h*-element results are those from calculating K_I directly using the domain integral procedure discussed in [31]. *P*-method results are obtained by first calculating J_I then solving for K_I. This is done rather than extracting K_I directly due to the error seen in Section 3.3.2. *P*-method results are shown for both plane stress and plane strain assumptions. It can be seen that near the plate's midplane the *h*-element results are similar to the *p*-element results when making a plane stress assumption. The *h*-element results approach the *p*-element plane strain assumption near the free surface. This could possibly be evidence that the crack is under plane stress conditions near the free surface and plane strain conditions closer to the center of the plate.

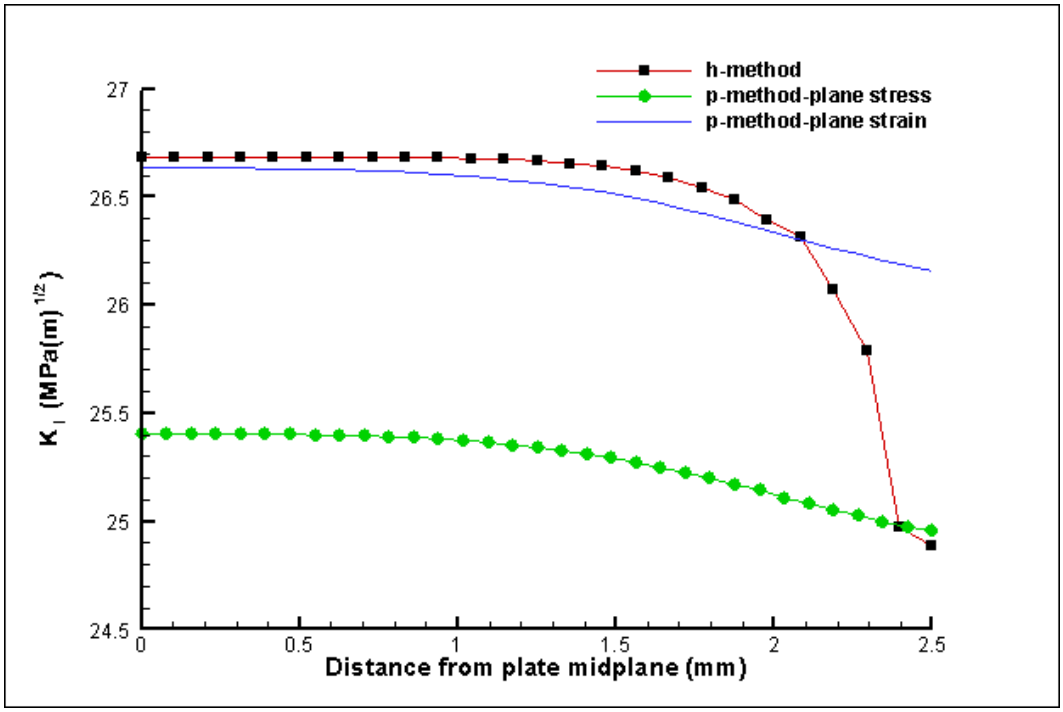

Figure 35: Comparison of refined results for 3D Models

The fact that the *p*-method is not correctly extracting K_I directly is a significant barrier to its use. The user is left to instead extract J_I and then calculate K_I using Equation 5 and Equation 6. Since the cracked area is generally under plane strain conditions but may transition to plane stress conditions near the free surface, the choice of using the plane strain or plane stress equation for this region must be made carefully.

3.5 Comparison of planar and three-dimensional results

Figure 36 compares the results for K_I for a 5mm thick plate. The *p*-element and *h*-element two-dimensional solutions give essentially the same result. These results however are significantly lower than the peak values obtained from the three-dimensional solutions near the plate mid-planes. The average three-dimensional solution at the plate midplane is 26.661 MPa·m$^{1/2}$. The average two-dimensional solution is 25.356 MPa·m$^{1/2}$. Assuming the three-dimensional solution is more correct at the plate's midplane, this is an error of 4.89 percent.

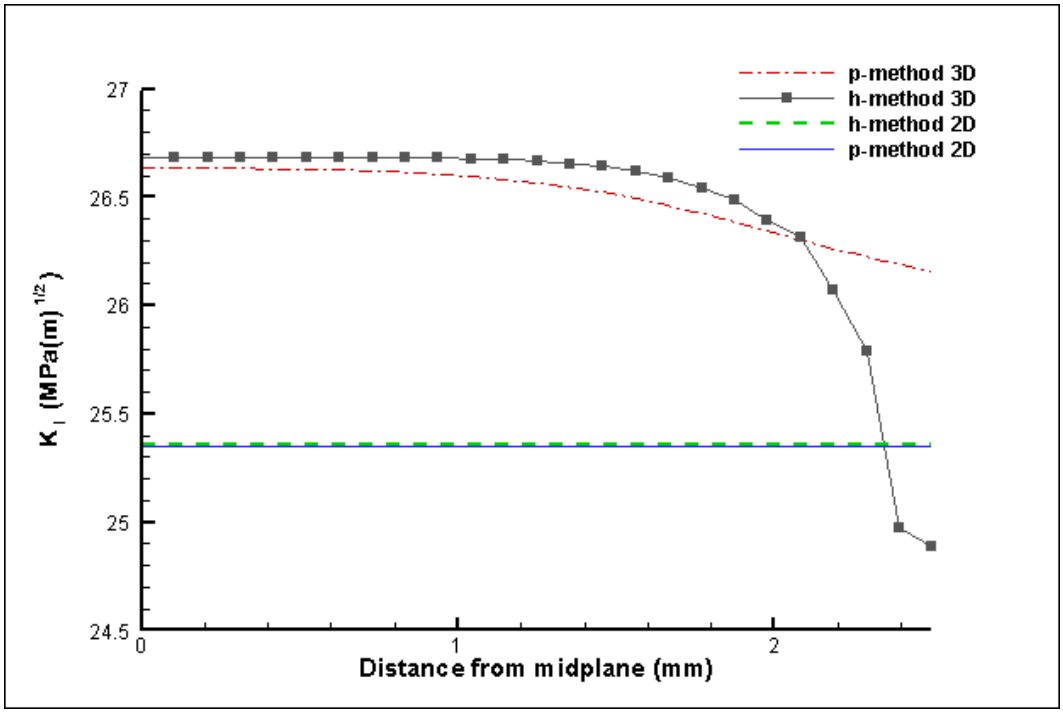

Figure 36: Comparison of K_I calculations for 5mm thick plate

3.6 Thickness effects on stress intensity factors

3.6.1 Three-dimensional analysis

H-element analysis

The refined *h*-method models labeled "Second Refinement" in Table 4 were modified in thickness to analyze K_I for different plate thicknesses. The same through-thickness density of twelve elements was used for the initial study. Figure 37 shows the result of this study. Figure 38 displays the same data, but with the plate thicknesses normalized to unity. These results show differences in behavior in the thicker models beginning at approximately three-quarters of the distance to the free surface, continuing to the free surface. Additional refinement was done as shown in Figure 39 to study this effect. The through-thickness mesh density near the midplane was kept the same as the

previously refined models, but the through-thickness density near the free surface was greatly increased. Table 5 summarizes the *h*-element mesh refinement.

Table 5: *H*-element mesh refinement with bias toward free surface

Configuration	Number of Elements	Number of Elements Through the Thickness	Mesh Bias
Second Refinement	56,100	12	none
Third Refinement	84,510	18	denser toward free surface

Results of this refinement for the 25mm thick plate are shown in Figure 40. The refinement resulted in three significant changes: 1) The maximum K_I was reduced through refinement 2) The stress intensity near the peak K_I became smoother 3) The minimum K_I near the free surface was reduced in value.

The remaining *h*-element models were given similar refinement. K_I values as a function of distance are shown in Figure 41, while normalized results are shown in Figure 42. It was seen that thicker models caused increasingly higher maximum K_I values. Also, as the model thickness was increased, the location of maximum K_I value moved from the plate midplane to a position just below the free surface.

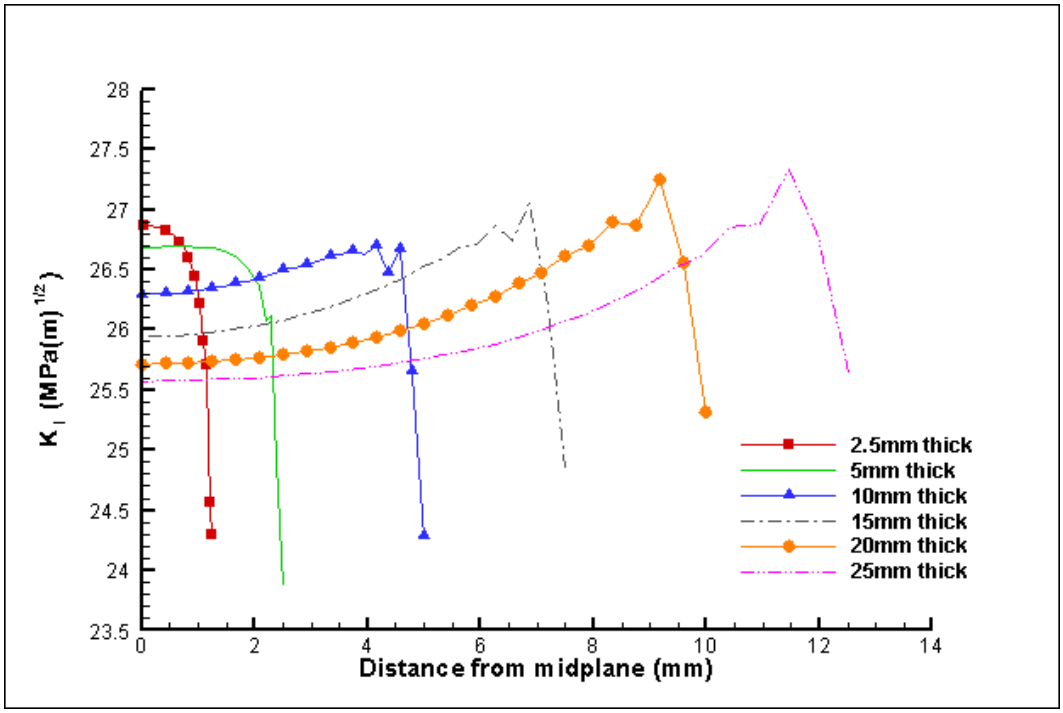

Figure 37: *H*-element analysis of different thickness plates

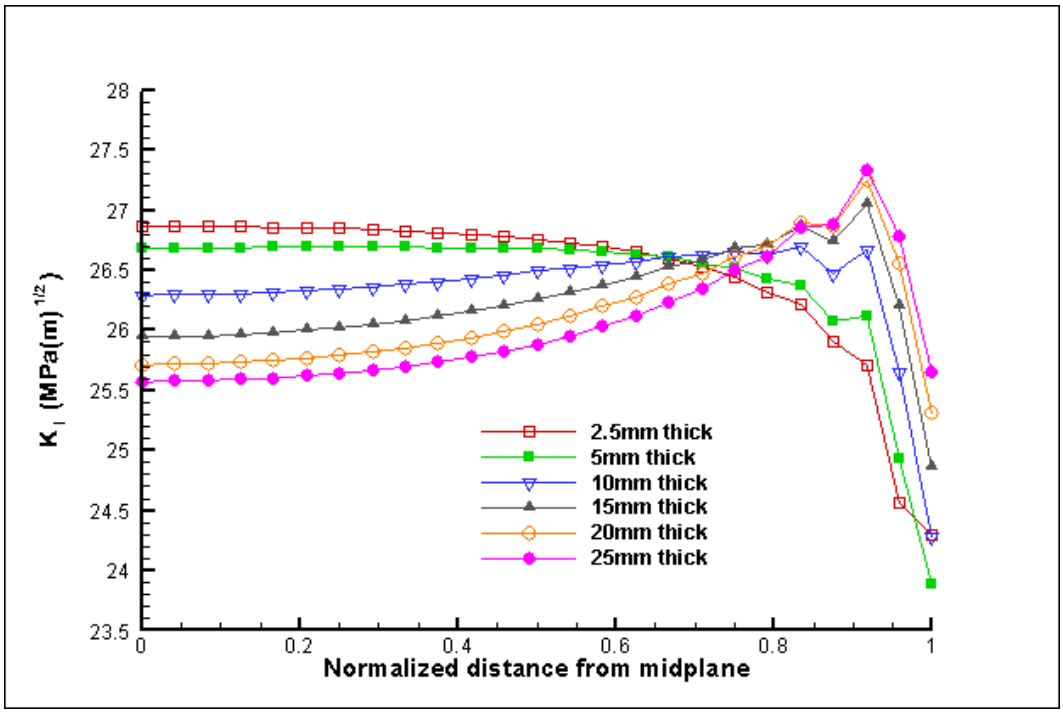

Figure 38: *H*-element results normalized for thickness

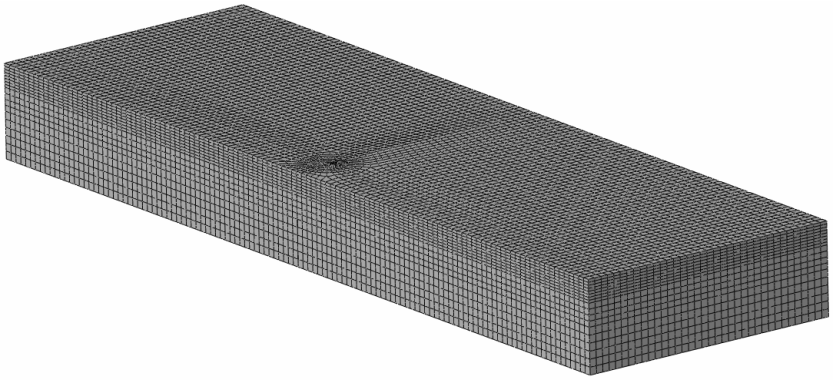

Figure 39: Refined Abaqus model of 25mm thick plate

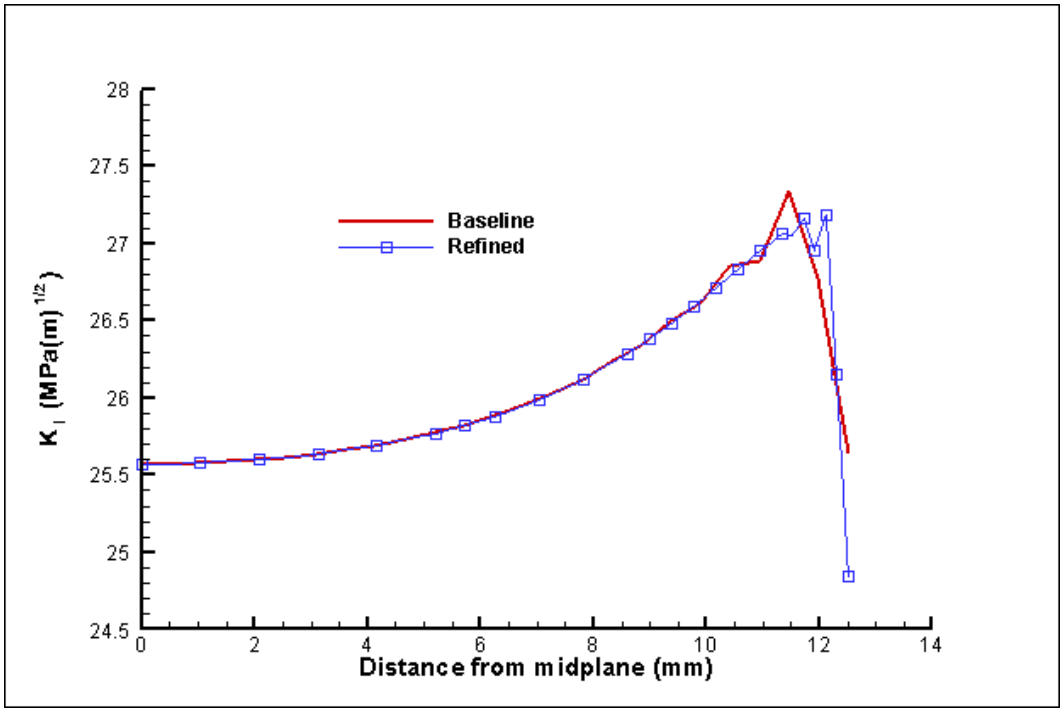

Figure 40: Refined results for 25mm thick plate

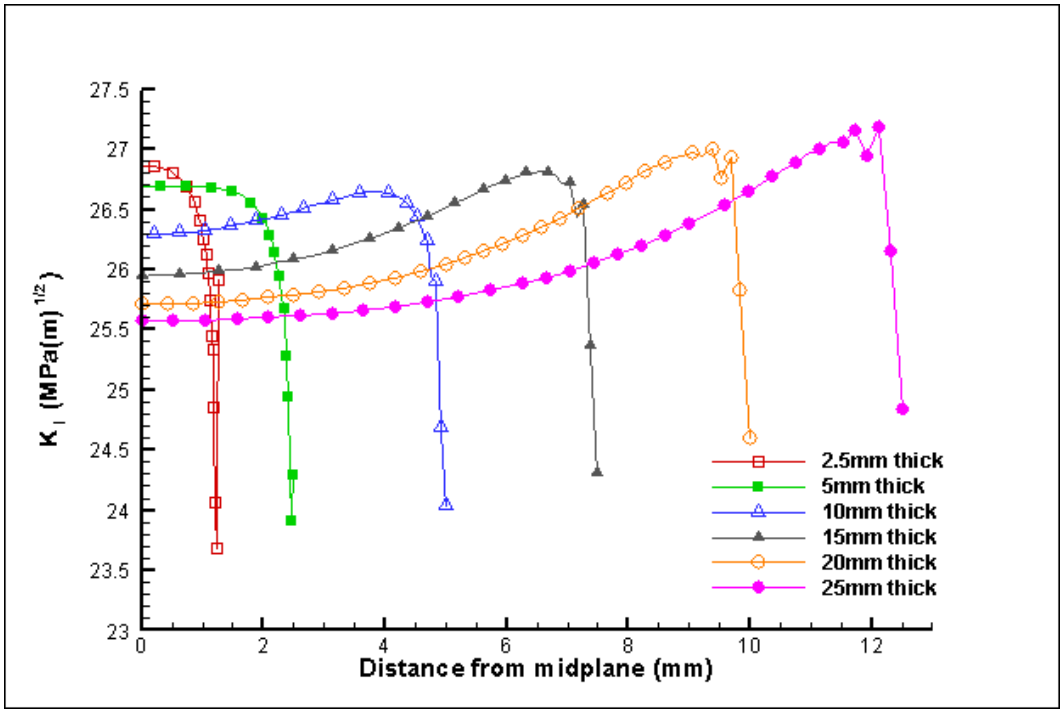

Figure 41: Refined *h*-element results as a function of distance

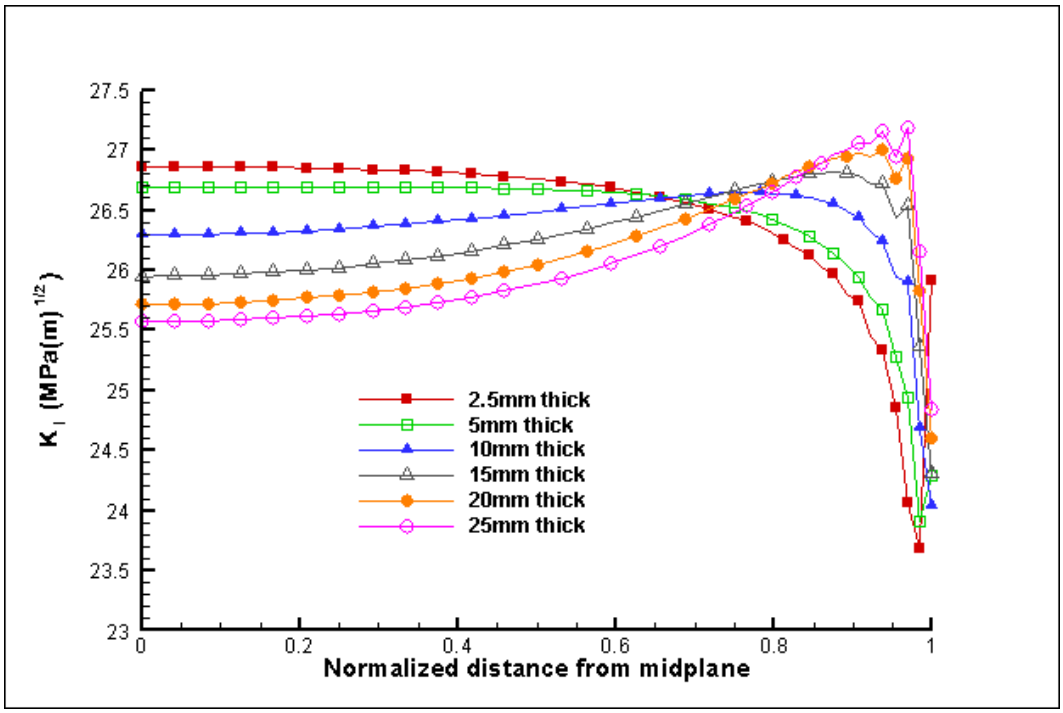

Figure 42: Refined *h*-element results normalized for distance

P-element analysis

The *p*-element model labeled "refined model" in Figure 33 was used for the following studies. The model thickness was changed for the six different studies, but the same mesh was used. Figure 43 shows the through-thickness variation in K_I for several different plate thicknesses. Figure 44 shows the variation normalized as a function of plate thickness percentage. It can be seen that for plates 5mm and less thick the Mode I stress intensity factor is highest at the plate midplanes. For plates 10mm thick and thicker, K_I is highest at a location slightly below the free surface. Figure 45 confirms that a converged solution was obtained.

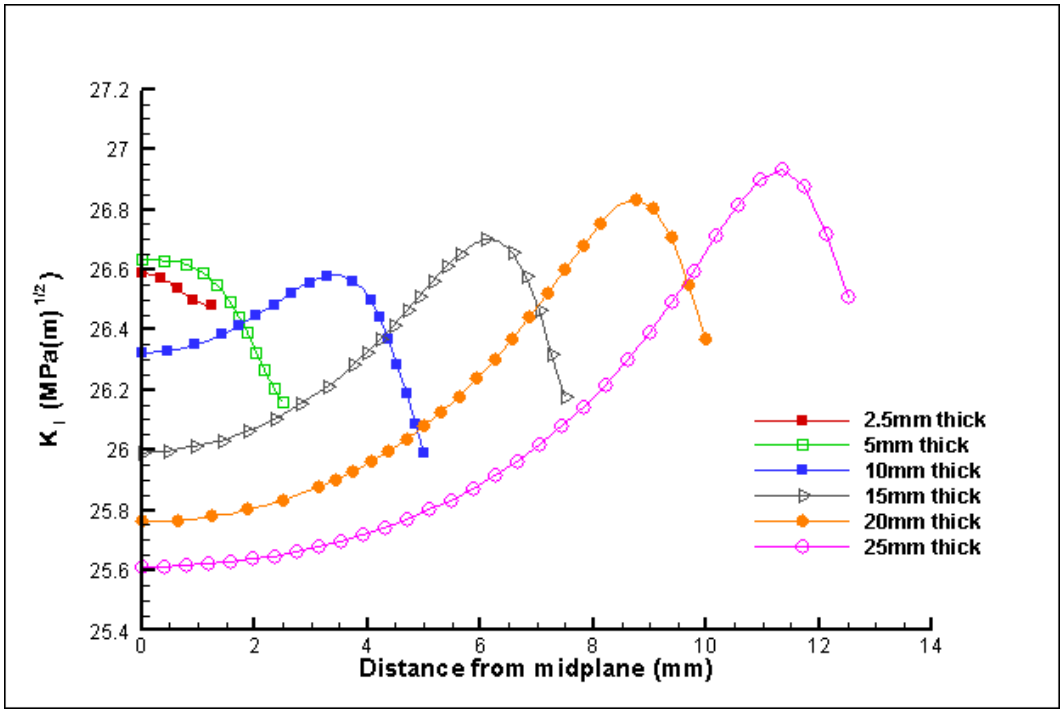

Figure 43: Through-thickness variation of K_I

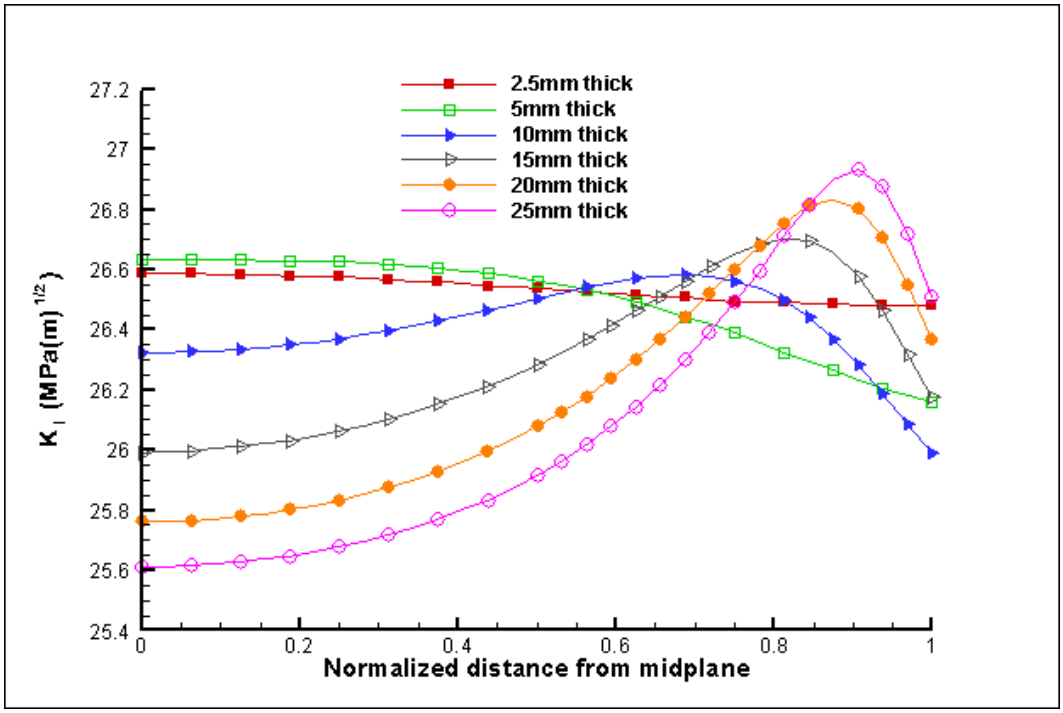

Figure 44: Normalized through-thickness variation of K_I

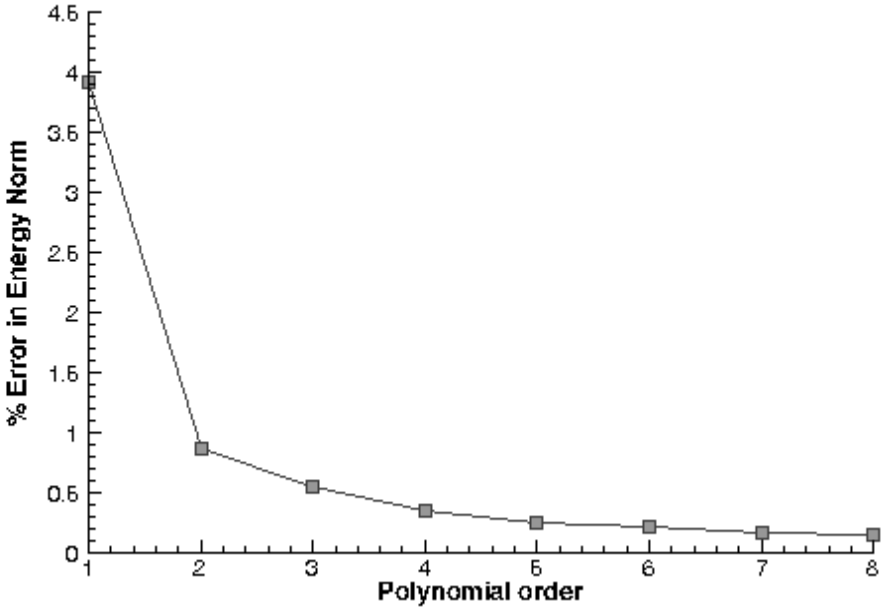

Figure 45: Convergence plot for 25mm thick *p*-element analysis

3.6.2 Comparison of methods, including two-dimensional analysis

The previously created two-dimensional models were modified and reran for the six plate thicknesses considered. The three-dimensional results from Section 3.6.1 were included for comparison. Results are shown in Figure 46Figure 46 through Figure 51.

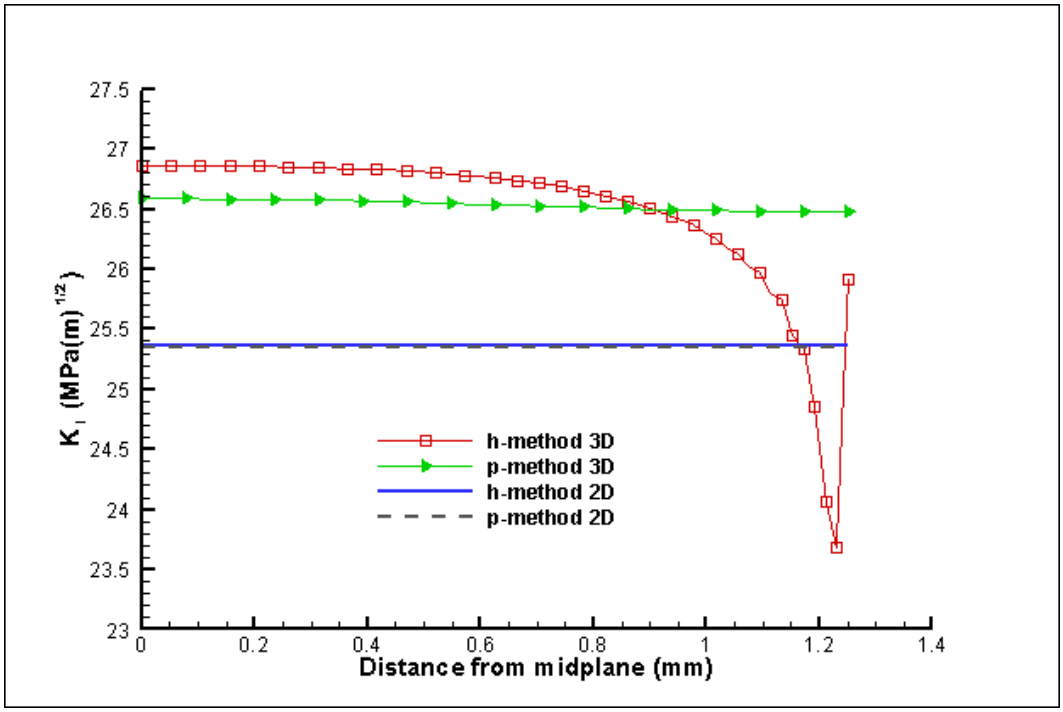

Figure 46: Comparison of methods for 2.5mm thick plate

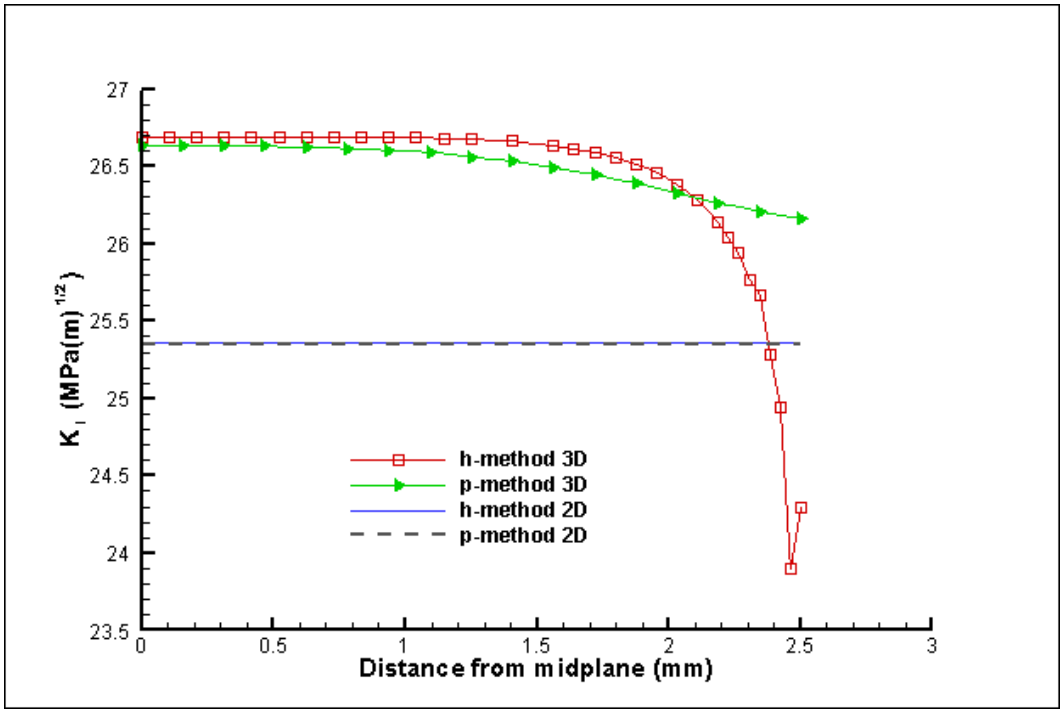

Figure 47: Comparison of methods for 5mm thick plate

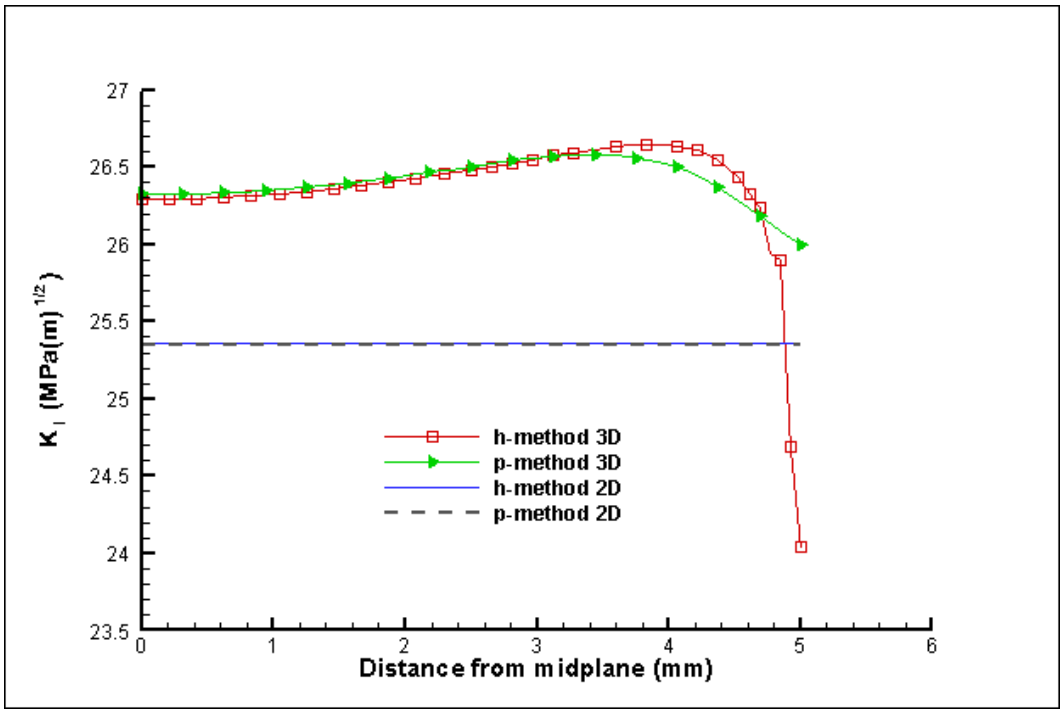

Figure 48: Comparison of methods for 10mm thick plate

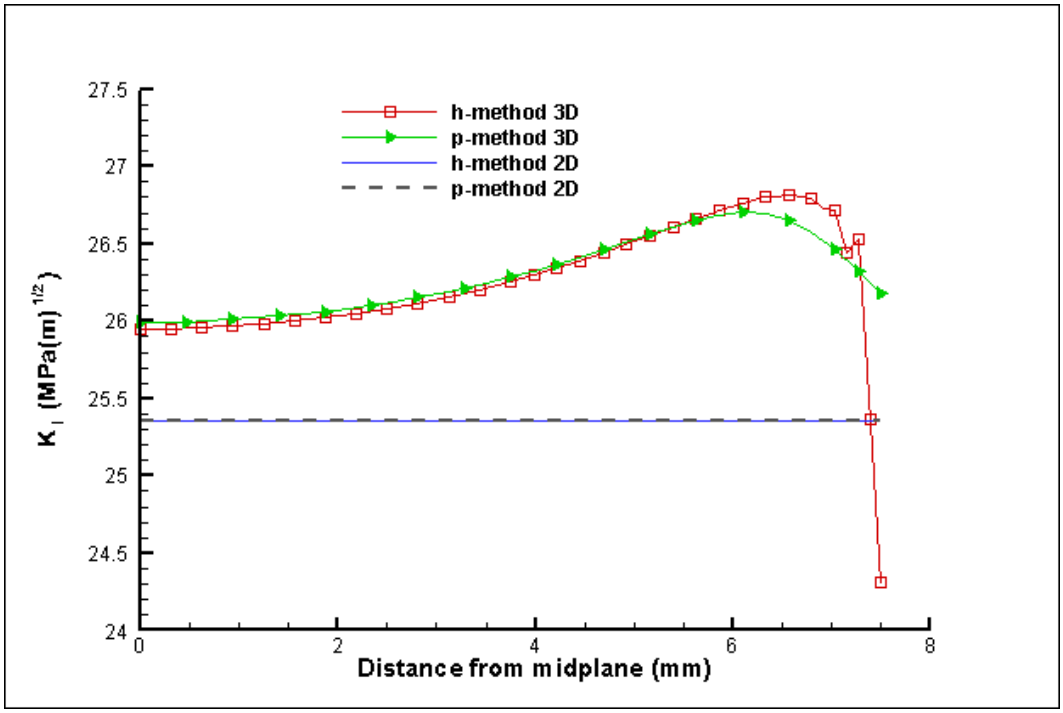

Figure 49: Comparison of methods for 15mm thick plate

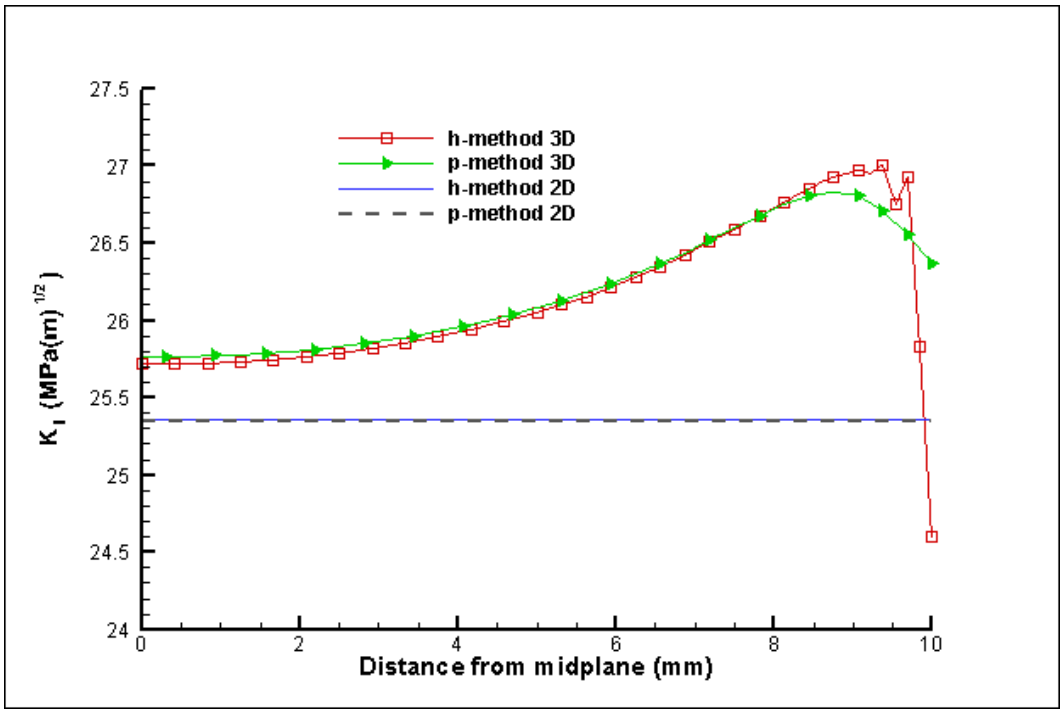

Figure 50: Comparison of methods for 20mm thick plate

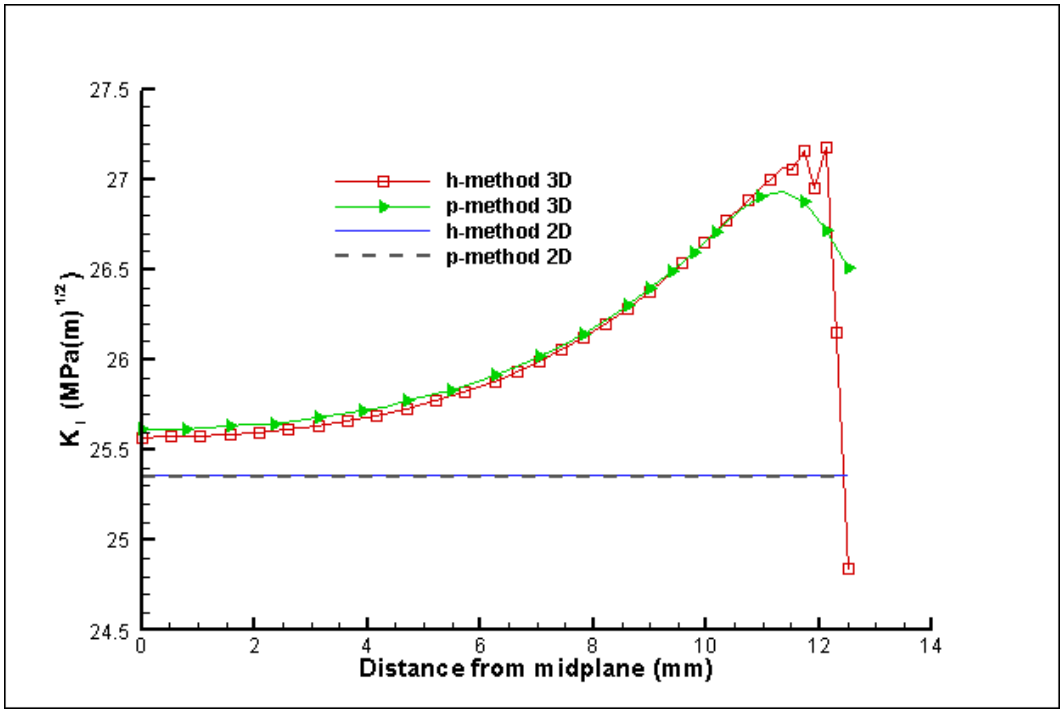

Figure 51: Comparison of methods for 25mm thick plate

It can be seen that the two-dimensional results are essentially equal for all thicknesses analyzed. The three-dimensional results are reasonably close to one another toward the center of the plate for the thicker specimens, but differ toward the free surfaces. Some of this variation may indicate the need for additional mesh refinement near the surface. Further studies would be needed to make this determination. For the thinner plates the *h*-method three-dimensional solution is slightly more conservative than the *p*-method three-dimensional solution toward the center of the plate. This is especially true for the 2.5mm thick plate. For all cases the three-dimensional results are more conservative than the two-dimensional results, except at the free surface. An analysis of the errors in the solutions is shown in Table 6. With the two-dimensional results essentially being identical, the average of the Abaqus and StressCheck results was used. For the three-dimensional results the maximum value obtained from the two three-

dimensional results was used, and was assumed to be the true maximum value. The error analysis was done accordingly.

Table 6: Error in using two-dimensional analysis

	K_I (MPa(m)$^{1/2}$)		
plate thickness	2D value	3D value	error, %
2.5 mm	25.356	26.865	5.6
5mm	25.356	26.691	5.0
10mm	25.356	26.643	4.8
15mm	25.356	26.816	5.4
20mm	25.356	27.003	6.1
25mm	25.356	27.181	6.7

For the plate thicknesses analyzed, the average error in K_I values associated with using a two-dimensional analysis is 5.6 percent. This compares well to Bakker [7] and Benthem's [19] previous work, where they estimate the error to be approximately 4.8 percent for the material used here.

3.7 Element type effects

All of the three-dimensional analysis within this research has been done using hexahedral (brick) and/or pentahedral (wedge) shaped elements. For StressCheck there is only one formulation available for these elements, which is fully integrated. This is because the *p*-elements do not suffer from Poisson's ratio locking like lower order elements may, and thus a reduced integration treatment is not necessary [32]. For the second-order solid elements used in the Abaqus three-dimensional models, there are three element integration schemes available. This is summarized in Table 7.

Table 7: Solid element types

Element Designation	*Solver*	*Description*
C3D20R	Abaqus	Reduced integration. Default element, reduces run time compared to C3D20 element.
C3D20	Abaqus	Fully integrated. May suffer from volumetric locking for nearly incompressible materials undergoing large strains.
C3D20H	Abaqus	Hybrid, linear pressure. Generally reserved for nearly incompressible materials.
Default	StressCheck	Fully integrated.

A study was done using the Abaqus model shown in Figure 39, which was modified to represent a five millimeter thick plate. The element formulation was changed and the corresponding through-thickness K_I values were recorded. The results of this study are shown in Figure 52.

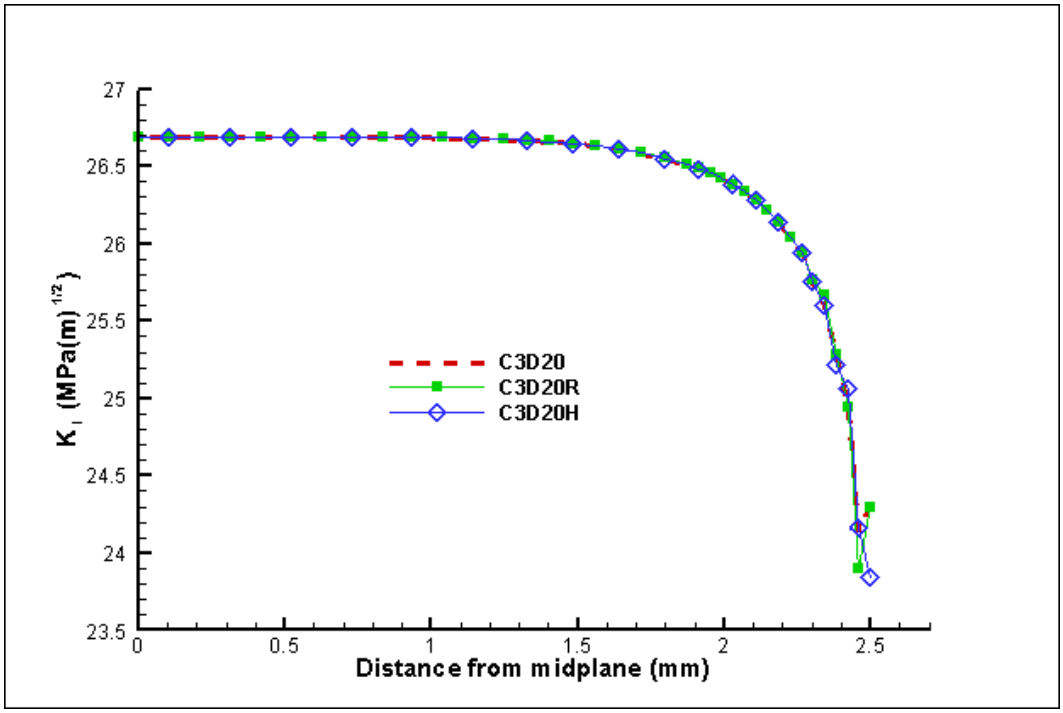

Figure 52: Comparison of element type on K_I extraction

Results for all three element types are nearly the same except for very near the free surface. Although normally reserved for (nearly) incompressible materials, the C3D20H (hybrid) elements appear to handle the end conditions better than either the C3D20 or C2D20R elements for the mesh used, assuming Benthem [19] is correct in his assertion that $K_I \rightarrow 0$ at the free surface. It is possible that this is because the volumetric strain varies linearly over the element for hybrid elements.

3.8 Effects of Poisson's ratio

A study was done to assess the error in using a two-dimensional planar analysis. The *p*-method was used to attain two- and three-dimensional solutions for three different Poisson's ratios, and two different plate thicknesses. Equation 8 is used to determine the predicted error. The actual error is calculated by assuming the maximum value of the three-dimensional solution is the true value, and then calculating the error between that

value and the two-dimensional value. Plots of K_I through the thickness of a 5mm thick plate and a 25mm thick plate are shown in Figure 53 and Figure 54, respectively. Table 8 compares the predicted and actual errors for the 5mm thick plate. Table 9 does the same for the 25mm thick plate. It can be seen that Equation 8 is accurate for the thin plate, but that the error in using planar analysis for a thicker plate is actually higher than the equation predicts.

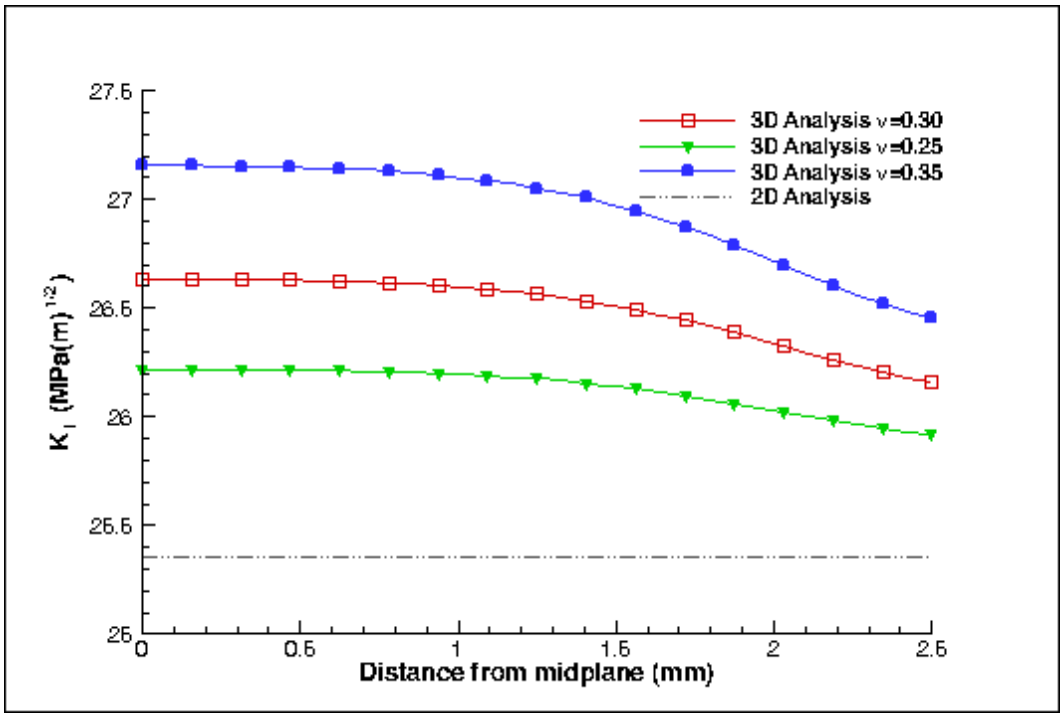

Figure 53: Through-thickness K_I for different ν for a 5mm thick plate

Table 8: Error in using planar analysis for a 5mm thick plate

Poisson's ratio	Predicted Error	Actual Error
0.25	3.28%	3.28%
0.30	4.83%	4.80%
0.35	6.75%	6.63%

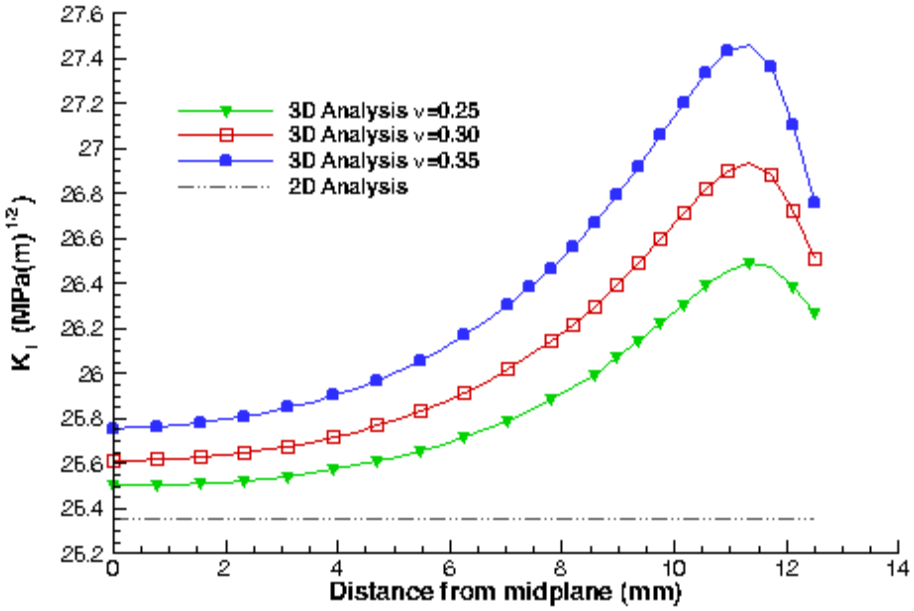

Figure 54: Through-thickness K_I for different ν for a 25mm thick plate

Table 9: Error in using planar analysis for a 25mm thick plate

Poisson's ratio	Predicted Error	Actual Error
0.25	3.28%	4.29%
0.30	4.83%	5.86%
0.35	6.75%	7.67%

4. Conclusions

4.1 Conclusions

The stress intensity factor is used in fracture mechanics to characterize the stress state near the crack tip in a structure under remotely applied loads. The magnitude of the stress intensity factor is dependent on geometry, the size and location of the crack, and

the magnitude and distribution of loads on the structure. The scope of this thesis is the study of the through-thickness stress intensity factor using two different FE approaches. *P*- and *h*-element finite element methods are used to study the stress intensity factors. The accuracy of the predicted Mode I stress-intensify factor (K_I) is assessed using closed-form and planar analysis approaches. The research also contains studies on how plate thickness, element formulations, and materials affect K_I, as well as possible relationships between the through-thickness K_I and K_C, the critical stress intensity factor.

Several conclusions may be made from this work:

1. The two methods of two-dimensional finite element analysis report nearly identical K_I values.
2. The two methods of three-dimensional finite element analysis report very close K_I values over approximately the center two-thirds of the plate, but differ closer to the free surface.
3. Two-dimensional analysis by its nature does not capture any variation of K_I through a plate's thickness. This results in a non-conservative outcome when compared to peak K_I values obtained from three-dimensional analysis. Additionally, the two-dimensional analysis is unable to capture the trend of K_I approaching zero at the free surface.
4. The theoretical error in using two-dimensional analysis given by Bakker [7] is confirmed for thin plates, but is actually higher than predicted for thicker plates.
5. The error associated with using two-dimensional analysis for calculating K_I is dependent on the plate material, and increases with increasing Poisson's ratio.

6. Using three-dimensional analysis, both the *h*-method and *p*-method report a peak K_I value at the midplane for the thinner specimens, specifically those that are 2.5 and 5mm thick. This is consistent with findings from the literature review [19] [8].
7. For specimens thicker than 5mm thick, both *h*- and *p*-methods predict a peak K_I value slightly below the free surface. This is consistent with Yamamoto's findings [8], and might be explained by Shivakumar's work on through-thickness singularities [21].
8. For the meshes used, the *h*-method models do a better job than the *p*-method models of approaching $K_I = 0$ at the free surface, as Benthem [19] reports should be the case at the free surface. It is assumed that if both mesh densities were increased infinitely, especially near the free surface, both would return the expected $K_I=0$ result at the free surface.
9. While the domain integral method used by Abaqus is somewhat insensitive to in-plane mesh density, it is very sensitive to through-thickness mesh density, particularly approaching the free surface.
10. The *p*-method appears to require significantly less mesh density near the free surface in order to adequately capture the peak K_I values that occur just below the free surface for thicker plates.
11. For modeling the through-thickness stress intensity factor using Abaqus, the C3D20H elements appear to provide the most stable results for capturing K_I near the free surface. It is possible that this is because hybrid elements force the volumetric strain to vary linearly over the element.

4.2 Suggestions for future research

Of particular interest for future work, partly because of a lack of such supporting research, is the rise of K_I just below the free surface for thicker specimens. Further, if this rise in K_I can be verified, the impact on this with regard to how it may tie into decreasing K_C with increasing plate thicknesses should be studied. The current ASTM standards [47] do have provisions for larger plate thicknesses to preclude plasticity near the crack tip; however, it may be not only plasticity that is responsible for the higher apparent toughness in thin plates. Also, more detailed mesh studies should be done to better determine what level of through-thickness mesh density is needed, especially near the free surface, to accurately capture the K_I gradient. In order to verify findings of this paper physical testing may be required. One of the methods discussed in Section 2.7.2 such as the frozen-stress technique or the multiple embedded grid moiré technique could be used for this. More mesh convergence studies would lead to a better understanding of accurate K_I extraction in cracked plates, especially in high gradient regions near the free surface of cracked plates.

5. References

[1] T.L. Anderson, *Fracture Mechanics Fundamentals and Applications*. 3rd Ed., Boca Raton, FL: Taylor & Francis, 2005.

[2] D. Tracey, "Finite Elements for Three-dimensional Elastic Crack Analysis," *Nuclear Engineering and Design*, vol. 26.2, pp. 282-290, 1974.

[3] G. Irwin, "Analysis of Stresses and Strains Near the End of a Crack Traversing a Plate," *Journal of Applied Mechanics*, vol. 24, pp. 361-364, 1957.

[4] H. Westergard, "Bearing Pressures and Cracks," *Journal of Applied Mechanics*, vol. 6, pp. 49-53, 1939.

[5] F. Beer and E. Johnston, *Mechanics of Materials*. 2nd Ed., New York, NY: McGraw-Hill, 1992.

[6] G. Sih, "A Review of the Three-dimensional Stress Problem for a Cracked Plate," *International Journal of Fracture Mechanics*, vol. 7.1, 1971.

[7] A. Bakker, "Three Dimensional Constraint Effects on Stress Intensity Distributions in Plate Geometries with Through-thickness Cracks," *Fatigue & Fracture of Engineering Materials & Structures*, vol. 15.11, pp. 1051-1069, 1992.

[8] Y. Yamamoto and Y. Sumi, "Stress Intensity Factors for Three-dimensional Cracks," *International Journal of Fatigue*, vol. 14.1, pp. 17-35, 1978.

[9] T. Nakamura and D. Parks, "Three-dimensional Crack Front Fields in a Thin Ductile Plate," *Journal of the Mechanics and Physics of solids*, vol. 38.6, pp. 787-812, 1990.

[10] "DTD Handbook," Lextech, Inc., 2011 <http://afgrow.net/applications/DTDHandbook>

[11] P. Paris and G. Sih, "Stress Analysis of Cracks," presented at 67th Annual Meeting of the American Society for Testing and Materials, 1965.

[12] E. Byskov, "The Calculation of Stress Intensity Factors Using the Finite Element Method with Cracked Elements," *International Journal of Fracture Mechanics*, vol. 26.4, pp. 329-337, 1984.

[13] A. Shukla and J.W. Dally, *Experimental Solid Mechanics*. Knoxville, TN: College House Enterprises, 2010.

[14] Z. Xian-Kui and J. Joyce, "Review of Fracture Toughness (G, K, J, CTOD, CTOA) Testing and Standardization," *Engineering Fracture Mechanics*, vol. 85, pp. 1-46, 2012.

[15] B. Szabó and I. Babuška, *Introduction to Finite Element Analysis*. West Sussex UK: Wiley, 2011.

[16] C.W. Smith, "Use of Photoelasticity to Obtain Stress-intensity Factors in Three-dimensional Cracked-body Problems." *Experimental Mechanics*, vol. 20.11, pp. 390-396, 1980.

[17] A. Ugural and S. Fenster, *Advanced Strength and Applied Elasticity*. 4th Ed., Upper Saddle River, NJ: Prentice Hall, 2008.

[18] A. Rosakis and K. Ravi-Chandar, "On Crack-tip Stress State: An Experimental Evaluation of Three-dimensional Effects," *International Journal of Solids and Structures*, vol. 22.2, pp. 121-134, 1986.

[19] J. Benthem, "The Quarter-infinite Crack in a Half Space; Alternative and Additional Solutions," *International Journal of Solids and Structures*, vol. 16.2, pp. 119-130, 1980.

[20] "Poisson's Ratio," *Wikipedia, The Free Encyclopedia*, Wikimedia Foundation, Inc., 2012. <http://en.wikipedia.org/wiki/Poisson's_ratio>

[21] K. Shivakumar and I. Raju, "Treatment of Singularities in Cracked Bodies," *International Journal of Fracture*, vol. 45, pp. 159-178, 1990.

[22] R. Hartranft and G. Sih, "An Approximate Three-dimensional Theory of Plates with Application to Crack Problems," *International Journal of Engineering Science*, vol 8, pp 711-729, 1970.

[23] *Mechanical APDL Structural Analysis Guide – version 14.0*, ANSYS, Inc., Cannonsburg, PA, 2011.

[24] *Abaqus Theory Manual – version 6.11*, Simulia, Providence, RI, 2011.

[25] *MSC.Nastran 2004 Reference Manual*, MSC.Software Corporation, Santa Ana, CA, 2004.

[26] I. Babuška and B. Szabó, "On the Rates of Convergence of the Finite Element Method," *International Journal for Numerical Methods in Engineering*, vol. 18, pp. 323-341, 1982.

[27] "PTC Creo Simulate Data Sheet," PTC, Needham, MA, 2012. <http://www.ptc.com/WCMS/files/128132/en/J0695_PTC_Creo_Simulate_DS_EN.pdf>

[28] H. Ozer, C. Duarte, and I. Al-Qadi, "Formulation and Implementation of a High-order 3-D Domain Integral Method for the Extraction of Energy Release Rates." *Computational Mechanics*, vol 49.4, pp. 459-476, 2012.

[29] H. De Lorenzi, "On the Energy Release Rate and the J-integral for 3-D Crack Configurations." *International Journal of Fracture*, vol 19, pp. 183-193, 1982.

[30] K. Shivakumar, P. Tan, and J. Newman, "A Virtual Crack-closure Technique for Calculating Stress Intensity Factors for Cracked Three Dimensional Bodies," *International Journal of Fracture*, vol. 36.3, 1988.

[31] *Abaqus Analysis User's Manual – version 6.11*, Simulia, Providence, RI, 2011.

[32] *StressCheck Master Guide, Release 9.0*, Engineering Software Research & Development, Inc., St. Louis, MO, 2009.

[33] B. Szabó and I. Babuška, *Finite Element Analysis*. New York, NY: 1991.

[34] "StressCheck Advanced Training in Elasticity Fracture Mechanics, Release 9.0," Engineering Software Research & Development, Inc., St. Louis, MO, 2009.

[35] J. Pereira and C. Duarte, "Extraction of Stress Intensity Factors from Generalized Finite Element Solutions," *Engineering Analysis with Boundary Elements*, vol. 29, pp. 397-413, 2005.

[36] P. Wen, M. Aliabadi, and D. Rooke, "A Contour Integral for Three-dimensional Crack Elastostatic Analysis," *Engineering Analysis with Boundary Elements*, vol. 20.2, pp. 101-111, 1997.

[37] S. McNeill, W. Peters, and M. Sutton, "Estimation of Stress Intensity Factor by Digital Image Correlation," *Engineering Fracture Mechanics*, vol. 28.1, pp. 101-112, 1987.

[38] B. Badalouka and G. Papadopoulos, "Experimental Evaluation of Stress-optical Constants by Caustics," *International Journal of Fracture*, vol. 171.1, pp. 85-90, 2011.

[39] G. Gao, Z. Li, and J. Xu, "Optical Method of Caustics Applied in Viscoelastic Fracture Analysis," *Optics and Lasers in Engineering*, vol. 49, pp. 632-639, 2011.

[40] K. Gong and Z. Li, "Caustics Method in Dynamics Fracture Problem of Orthotropic Materials," *Optics and Lasers in Engineering*, vol. 46, pp. 614-619, 2008.

[41] H. Tippur, "Coherent Gradient Sensing (CGS) Method for Fracture Mechanics: A Review," *Fatigue & Fracture of Engineering Materials & Structures*, vol. 33.12, pp. 832-858, 2010.

[42] T. Chu, W. Ranson, M. Sutton, "Applications of Digital-image-correlation Techniques to Experimental Mechanics," *Experimental Mechanics*, vol. 25.3, pp. 232-244, 1985.

[43] T. Beckwith, R. Marangoni, and J. Lienhard, *Mechanical Measurements*. 5th Ed., Reading, MA: Addison-Wesley, 1993.

[44] S. Dhar, G. Cloud, and S. Paleebut, "Measurement of Three-dimensional Mode-I Stress Intensity Factor Using Multiple Embedded Moire Technique," *Theoretical and Applied Fracture Mechanics*, vol. 12.2, pp. 141-147, 1989.

[45] J. Cemosek, "Three-dimensional Photoelasticity by Stress Freezing," *Experimental Mechanics*, vol. 20.12, pp. 417-426, 1980.

[46] J. Cemosek, "Material for Casting Three-dimensional Photoelastic Models," *Experimental Mechanics*, vol. 30.3, pp. 258-263, 1990.

[47] ASTM Standard E399-09e2, "Standard Test Method for Linear-elastic Plane-strain Fracture Toughness Ic of Metallic Materials," ASTM International, West Conshohocken, PA, 2011.